Research on Distance Protection Scheme for Single-phase to Ground Faults in Active Distribution Networks with Gap-grounded Transformers

Wanqi Yuan, Yongli Li, *Member*, *IEEE*, Xiaolong Chen, *Member*, *IEEE*, Shaofan Zhang, Jing Wan, and Huili Tian

***Abstract*—When a single-phase to ground fault (SPGF) occurs near the main power source in an active distribution network, distance protection section II (DPS-II) located at the distributed generator (DG) side operates with a delay. In gap-grounded transformers, this delay can lead to gap breakdown due to neutral-point overvoltage, which adversely affects the operation of DPS-II on the DG side. To address this issue, this paper proposes an improved DPS designed for active distribution networks with gap-grounded transformers. First, the factors influencing the additional impedance are analyzed after gap breakdown. To mitigate the effects of the additional impedance on DPS performance, an improved DPS based on real short-circuit impedances is introduced for active distribution networks. This scheme utilizes the negative-sequence current distribution factor on the DG side to accurately calculate the additional impedance angle, ensuring reliable protection. Simulation results demonstrate that the proposed scheme effectively operates under forward faults across various DG capacities, fault locations, local loads, and fault transition resistances. In addition, it avoids tripping under reverse faults, thereby confirming its reliability and superiority.**

***Index Terms*—Distributed generator (DG), gap breakdown, distance protection section II (DPS-II), additional impedance, real short-circuit impedance.**

I. Introduction

Distance protection is widely employed in 110 kV transmission lines due to its high sensitivity and low vulnerability to variations in grid operation conditions. For single-phase to ground faults (SPGF) on the transmission lines, distributed generators (DGs) connected to gap-grounded transformers can disrupt protection operation. If a SPGF occurs in proximity to the main power source, the distance protection section I (DPS-I) can promptly initiate a trip, whereas the operation of DPS-II at the DG side encounters a delay [1]–[3]. During the delay period, the neutral-point gap of the transformer is likely to collapse, altering the zero-sequence network of the system and generating zero-sequence current. Thus, the current measured by the impedance relay includes the zero-sequence component flowing through the protection point [4], [5]. As a result, the operational effectiveness of the DPS-II on the DG side is compromised by the gap breakdown.

Currently, there are limited researches on the issue of gap breakdown in transformers. The neutral-point voltage after an SPGF when different types of DGs are connected to the distribution network in investigated in [6]. While the authors propose suggestions to prevent the gap breakdown issue, the analysis of the neutral-point voltage after the tripping of the transmission line protection is not considered. In [7], the neutral-point voltage after the tripping of the line protection is studied, which confirms that gap breakdown occurs in the event of imbalance between the DG capacity and local load. However, the influence of gap breakdown on the performance of the distance protection scheme (DPS) is ignored in the study.

To improve DPS performance, some studies have proposed adaptive protection setting methods based on grid operation modes and fault information [8]–[10]. In [11], the simulation results in various grid operation modes are used as samples, and DPS performance is obtained through offline training using artificial intelligence algorithms. The active components, reactive

Received: October 16, 2024
Accepted: February 1, 2025
Published Online: September 1, 2025
Wanqi Yuan, Yongli Li (corresponding author), and Xiaolong Chen are with the School of Electrical and Information Engineering, Tianjin University, Tianjin 300110, China (e-mail: 18861821151@163.com; lyltju@163.com; xiaolong.chen@tju.edu.cn).
Shaofan Zhang, Jing Wan, and Huili Tian are with Guangzhou Power Supply Bureau, Guangdong Power Grid Co., Ltd., Guangzhou 510630, China (e-mail: bbgl_gz@163.com; epwanj@163.com; tianhuili2011@163.com).
DOI: 10.23919/PCMP.2024.000287

components, and transition resistances are input into the deep learning model [12], and the protection action range is adjusted by utilizing the output values of the radial basis function neural network. A DPS using measured impedance trajectory as a weight coefficient is proposed in [13], where a current auxiliary criterion is introduced to improve the speed of DPS. However, the study based on intelligence algorithms requires substantial simulation experiments and calculations. In addition, the action performance is determined by the number of samples, whereas it is challenging to utilize all samples during the offline training to adapt to the complex grid operation modes and massive fault information in new power systems.

Researchers have investigated DPS based on impedance and voltage phasor planes, as the voltage phasor plane can effectively reflect the fault characteristics of the transmission lines. The voltage drops between the protection location and fault point are calculated based on the phasor relationship between the measured voltage and fault-point voltage to establish the distance protection criterion [14], [15]. In [16], the forward faults and reverse faults are distinguished based on the voltage distribution tendency in the transmission line. In [17] and [18], fault currents are estimated using the sequence currents at the fault locations, while bivariate linear equations of the fault locations and transition resistances are established based on measured impedance. Subsequently, DPS is realized to alleviate the effects of the transition resistances. Other studies have broadened DPS based on the plural impedance plane. Based on the load and short-circuit currents during the fault period, reference [19] solves the reactance between the fault point and protection location using a DPS-I scheme. Based on the geometric relationships in the plural impedance plane, the real short-circuit impedances between the fault point and protection locations are acquired [20]–[22]. Nevertheless, DPS at the DG sides in a gap-grounded system is inadequate in these studies. An improved DPS-II scheme based on the self-hold signal and zero-sequence current in a gap-grounded system is proposed in [23]. However, it simply attributes the failure of DPS-II to gap breakdown without analyzing the factors affecting the DPS performance.

In a gap-grounded system, when an SPGF occurs on the transmission line, it is crucial for DPS-I at the main power source and on the DG side to respond rapidly, thereby removing the fault and preventing prevent gap breakdown. If the SPGF is located near the main power source side, DPS-II on the DG side operates with a delay. During this delay, the system grounding mode is altered by the gap breakdown, which degrades the reliability of DPS on the DG side. In the event of a gap breakdown, a zero-sequence circuit is established between the fault location and transformer neutral point, resulting in the generation of a zero-sequence current in the gap-grounded system. It is widely acknowledged that the measured current in grounding distance protection comprises both the fault-phase current and zero-sequence current. Therefore, DPS on the DG side may fail to operate in this scenario.

To solve this issue, this study makes the following contributions.

1) The grounding mode of the neutral point strongly affects the DPS performance. The DPS performance is first discussed for a gap-grounded system following a gap breakdown by referring to existing studies.

2) The failure mechanism of DPS-II on the DG side is analyzed in the gap-grounded system. Following the gap breakdown, the measured impedance at the protection location on the DG side is confirmed to correlate with the DG capacity.

3) For single-DG and multiple-DG networks, an improved DPS is proposed based on the relationship between the impedance phasors in the directional impedance circle. By employing the sine theorem of triangles, the real short-circuit impedance expression can be derived using the measured impedance and distance protection parameters.

4) To distinguish reverse and forward faults, a fault-phase current criterion based on the fault current at the protection location on the DG side is proposed for a single-DG network. In a multiple-DG network, the distance protection parameter is calculated to be negative in order to identify reverse faults.

The remainder of this paper is organized as follows. The graded insulation level of the transformer and T-type network are introduced in Section II, while the derivation of the real short-circuit impedance is presented in Section III. Simulation results and conclusion are presented in Sections IV and V, respectively.

II. System Model and the Measured Impedance Analysis

The relay protection regulations stipulate that the neutral point of a 110 kV transformer should adopt a solid grounding mode. However, in the real-world operation of power grids, some of the neutral points of 110 kV transformers are ungrounded, whereas the others are directly grounded. For ungrounded transformers, spark gaps and protection devices are usually installed at the neutral points.

Gap-grounded transformers are frequently employed in the T-type wiring distribution networks of certain cities in China [24], [25]. With the integration of DGs, distance protection should be configured on the high-voltage side of 110/10 kV transformers, rather than solely on the main power source side [26], [27]. As stated in Section I, the protection action at the main power source side affects the neutral-point voltage, potentially leading to gap breakdown in severe instances. Hence, the fault characteristics of a T-type network with gap-grounded transformers requires urgent analysis.

A. T-type Wiring Active Distribution Network

The T-type wiring networks of a 110 kV transmission line with DGs are illustrated in Fig. 1. In traditional passive distribution networks, distance protection is implemented only on the system side. However, with the development of new power systems, distance protection on the DG side is gradually being introduced.

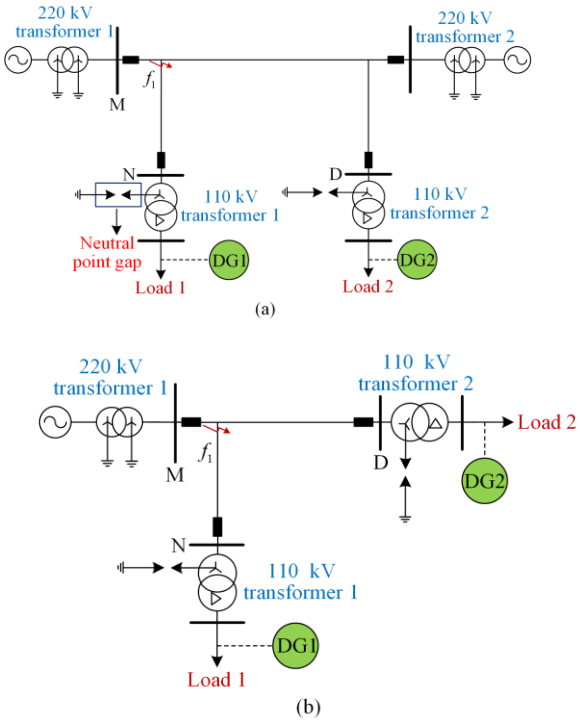

Fig. 1. 110 kV transmission line of a T-type distribution networks with DGs. (a) Double main power sources. (b) Single main power source.

Figure 1 shows two T-type wiring networks: single main power source and double main power sources. Gap-grounded transformers from two 110 kV substations are linked to the 110 kV transmission lines. DGs are connected to the low-voltage side of the transformers, and distance protection is configured on both sides of the main power source and DGs. An SPGF f_1 occurs near the forward area of the protection at bus M in Fig. 1, i.e., the protection range of DPS-I on the side of bus M and that of DPS-II on the side of bus N or D. Subsequently, DPS-I on the side of bus M promptly responds, whereas that on the side of bus N or D does not operate. Typically, the protection range of DPS-I is 80% of the transmission line, with the remaining 20% requiring DPS-II intervention to clear the faults. To ensure reliability and selectivity, DPS-II on the DG side is set to operate after a delay (300–500 ms).

During the delay, if there are DGs on the low-voltage side, the neutral points of the 110 kV transformers may experience overvoltage owing to the power imbalance between the DG capacities and local loads [7]. When the neutral-point voltage exceeds the withstand voltage of the transformer insulation, neutral-point gap breakdown can occur. Typically, the graded insulation levels of 110 kV transformers are 35 kV, 44 kV, and 60 kV [28]. As shown in Table I, the graded insulation levels have different power frequency withstand voltages.

TABLE I
DIFFERENT GRADED INSULATION LEVELS

Insulation level (kV)	RMS values of withstand voltage (kV)	
	Ignore safe parameter	Consider safe parameter
35	85	72.25
44	95	80.75
66	140	119

Table I indicates that as the insulation level increases, the withstand voltage value rises by a significant extent. A safety parameter of 0.85 is selected by considering factors such as the transformer's age, temperature, humidity, and environmental conditions. Under normal grid operation, the neutral-point voltage has no offset. However, following a fault f_1 in Fig. 1, the neutral-point voltage is deviated due to the asymmetric three-phase voltage. Subsequently, the protection action of the main power source side causes the DGs to be disconnected from the grid. In this instance, the neutral-point overvoltage probably stems from the power imbalance. If the neutral-point voltage exceeds its withstand voltage, neutral-point gap breakdown occurs instantaneously within microseconds.

However, the neutral-point voltages are different between Figs. 1(a) and (b) during the delay. In Fig. 1(a), the DGs remain connected to the grid after the protection at bus M trips, so the neutral-point voltage is unrelated to the low-voltage side of the 110 kV transformer. Instead, it depends on the line impedance and rated phase voltage on the high-voltage side, which is lower than the gap breakdown voltage. This implies that gap breakdown issue does not occur in the double power source system. Therefore, the distance protection on the DG side will not be affected by the gap-grounded system. In contrast, after the DGs are disconnected from the single power source system, gap breakdown issue may occur due to power imbalance between the local load and DGs [29]. When the gap is broken down, the neutral point is grounded, allowing a zero-sequence current to flow through the protection location. The measured current and impedance are subsequently altered, and the reliability of DPS-II is reduced. Therefore, this study aims to investigate the performance of DPS-II in a single power source system under SPGFs.

Based on Fig. 1(b), the rated capacity of the DG is set as 10 MW, and the local load varies between 1 MW, 2 MW, 4 MW, and 5 MW to observe the neutral-point $\dot{U}_{n0}$. Figure 2 displays the $\dot{U}_{n0}$ with different trans-

former insulation levels. An SPGF occurs at 2 s, and the circuit breaker on the side of the system trips at 2.1 s.

In Fig. 2, the gap breakdown times are all within 13 ms. Specifically, the graded insulation level is 60 kV in Fig. 2(c) and its withstand voltage is 119 kV. The neutral-point gaps are safe for $P_L = 4$ MW and 5 MW, showcasing a high tolerance for overvoltage at the 60 kV insulation level. Notably, the gap breakdown occurs prior to the operation of DPS-II.

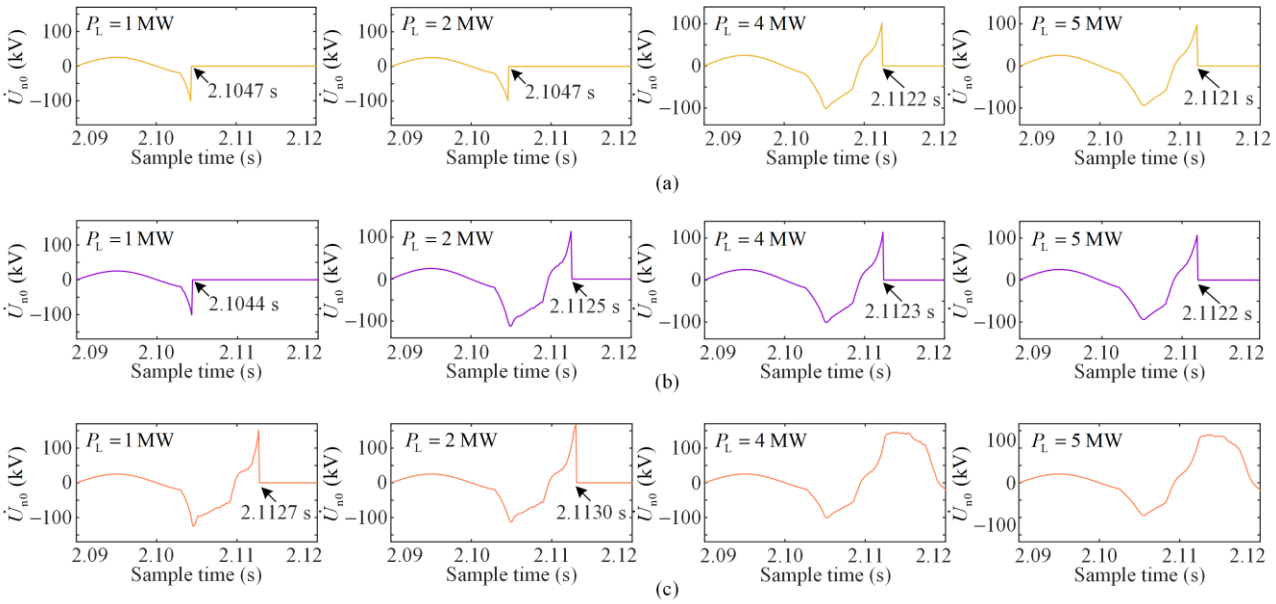

Fig. 2. Neutral-point voltage with different graded insulation levels of transformer. (a) Insulation level: 35 kV. (b) Insulation level: 44 kV. (c) Insulation level: 66 kV.

Moreover, the measured current for the grounding distance protection comprises the fault-phase current and zero-sequence current. Because the neutral point is directly grounded after the gap breakdown, the zero-sequence current distribution and measured current are subsequently altered. Thus, gap breakdown clearly affects the reliability of DPS.

B. Measured Impedance Analysis on the DG Side

Based on electricity demands, DGs are randomly integrated into the low-voltage side of a 110/10 kV transformer. The objective of this study is to comprehensively evaluate the measured impedances on the DG side of T-type networks featuring both single and multiple DGs.

1) Measured Impedance in a T-type network with Single DG

Assume that the SPGF occurs at the beginning of line MN in Fig. 1(b) at phase A. The fault transition resistance is R_f, and the short-circuit current distribution is shown in Fig. 3, where $\dot{E}_s$ is the system source; $\dot{I}_{DG}$ is the short-circuit current output by the DG, $\dot{I}_N$ is the measured current at QF2; $\dot{I}_{gapN}$ is the gap zero-sequence current on the reverse side of QF2; and $\dot{I}_f$ is the fault-point current.

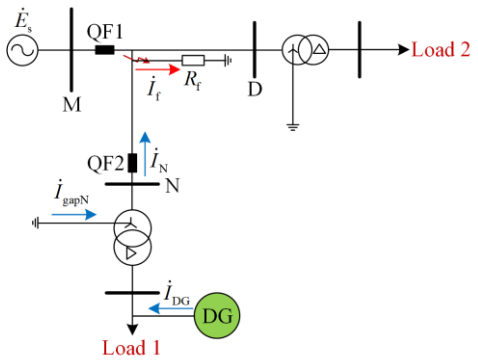

Fig. 3. Short-circuit current distribution in a T-type network with a single DG.

The SPGF in the forward region of line MN triggers the immediate tripping of QF1. Subsequently, the network is transformed from double power sources to a single power source. Simultaneously, the fault persists in the transmission line, leading to an asymmetry in the three-phase voltages. Consistent offsets of the neutral-point voltages are observed in all the gap-grounded transformers. After gap breakdown, the neutral points are grounded, forming a zero-sequence network between the fault point and neutral point. Because there is no DG on the Load 2 branch, distance protection is only set up at bus N. Therefore, the measured impedance at QF2 can be represented as [30]:

$$Z_{\mathrm{N}}=\frac{\dot{U}_{\mathrm{N}}}{\dot{I}_{\mathrm{N}}}=\frac{\dot{I}_{\mathrm{N}}Z_{\mathrm{MN(1)}}+\dot{I}_{\mathrm{f}}R_{\mathrm{f}}}{\dot{I}_{\mathrm{N}}}=Z_{\mathrm{MN(1)}}+\frac{\dot{I}_{\mathrm{f}}}{\dot{I}_{\mathrm{N}}}R_{\mathrm{f}}=\underbrace{Z_{\mathrm{MN(1)}}}_{\text{Real short-circuit impedance}}+\underbrace{\frac{\dot{I}_{\mathrm{f.A}}}{\dot{I}_{\mathrm{N.A}}+3k_{\mathrm{MN}}\dot{I}_{\mathrm{N(0)}}}R_{\mathrm{f}}}_{\text{Additional impedance}} \tag{1}$$

where $k_{\mathrm{MN}}=(Z_{\mathrm{MN(1)}}-Z_{\mathrm{MN(0)}})/3Z_{\mathrm{MN(1)}}$ is a zero-sequence current compensation parameter; while $Z_{\mathrm{MN(1)}}$ and $Z_{\mathrm{MN(0)}}$ are the positive-sequence impedance and zero-sequence impedance of line MN, respectively; k_{MN} can be considered as a constant, as the line impedance is relatively steady, and k_{MN} is set to 2/3 in this study; $\dot{U}_{\mathrm{N}}$ is the measured voltage at QF2; Z_{N} is the measured impedance at QF2; $\dot{I}_{\mathrm{N.A}}$ is the short-circuit current of phase A at QF2; and $\dot{I}_{\mathrm{f.A}}$ is the fault point current of phase A. In (1), Z_{N} comprises the real short-circuit impedance $Z_{\mathrm{MN(1)}}$ and an additional impedance $(\dot{I}_{\mathrm{f}}/\dot{I}_{\mathrm{N}})R_{\mathrm{f}}$. It can be concluded that $Z_{\mathrm{MN(1)}}$ is stable for a known fault and $(\dot{I}_{\mathrm{f}}/\dot{I}_{\mathrm{N}})R_{\mathrm{f}}$ is dominated by $\dot{I}_{\mathrm{N(0)}}$, $\dot{I}_{\mathrm{N.A}}$, $\dot{I}_{\mathrm{f.A}}$, and R_{f}. Based on the boundary conditions for SPGFs [31], there is:

$$\dot{I}_{\mathrm{f.A}}=\dot{I}_{\mathrm{N.A}}=3\dot{I}_{\mathrm{N(0)}} \tag{2}$$

For a single-DG network, the amplitudes and angles of $\dot{I}_{\mathrm{f.A}}$, $\dot{I}_{\mathrm{N.A}}$, and $3\dot{I}_{\mathrm{N(0)}}$ in (2) are theoretically equivalent. Hence, Z_{N} and $(\dot{I}_{\mathrm{f}}/\dot{I}_{\mathrm{N}})R_{\mathrm{f}}$ are mainly determined by R_{f}. The additional impedance $(\dot{I}_{\mathrm{f}}/\dot{I}_{\mathrm{N}})R_{\mathrm{f}}$ is resistive, and QF2 is likely to fail to trip for a high transition resistance fault.

2) Measured Impedance in a T-type Network with Multiple DGs

In the scenario involving multiple DGs linked to the grid, the distribution of short-circuit currents is depicted in Fig. 4.

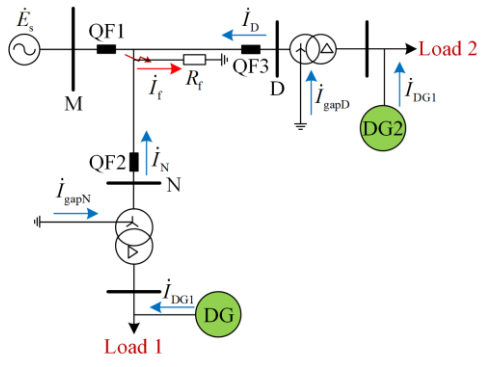

Fig. 4. Short-circuit current distribution for a T-type network with multiple DGs.

In the multiple-DG network, distance protections are configured at the high-voltage sides of the two 110/10 kV transformers. When the SPGF occurs in the forward region of QF1, it promptly trips. Then, three-phase asymmetrical voltages exist along the transmission line. The voltages at the neutral points are primarily influenced by the DGs and loads at the low-voltage sides of the 110 kV transformers, and gap breakdowns occur simultaneously. Subsequently, the neutral points are grounded, and zero-sequence currents flow through QF2 and QF3. In Fig. 4, $\dot{I}_{\mathrm{DG1}}$ and $\dot{I}_{\mathrm{DG2}}$ are the output short-circuit currents of DG1 and DG2, $\dot{I}_{\mathrm{D}}$ is the measured current at QF3, and $\dot{I}_{\mathrm{gapD}}$ is the gap zero-sequence current on the reverse side of QF3.

Similarly, the measured impedances at QF2 and QF3 are expressed as:

$$\begin{cases} Z_{\mathrm{N}}=\dfrac{\dot{U}_{\mathrm{N}}}{\dot{I}_{\mathrm{N}}}=\dfrac{\dot{I}_{\mathrm{N}}Z_{\mathrm{MN(1)}}+\dot{I}_{\mathrm{f}}R_{\mathrm{f}}}{\dot{I}_{\mathrm{N}}}=Z_{\mathrm{MN(1)}}+\dfrac{\dot{I}_{\mathrm{f}}}{\dot{I}_{\mathrm{N}}}R_{\mathrm{f}}= \\ \qquad Z_{\mathrm{MN(1)}}+\dfrac{\dot{I}_{\mathrm{f.A}}}{\dot{I}_{\mathrm{N.A}}+3k_{\mathrm{MN}}\dot{I}_{\mathrm{N(0)}}}R_{\mathrm{f}} \\ Z_{\mathrm{D}}=\dfrac{\dot{U}_{\mathrm{D}}}{\dot{I}_{\mathrm{D}}}=\dfrac{\dot{I}_{\mathrm{D}}Z_{\mathrm{DM(1)}}+\dot{I}_{\mathrm{f}}R_{\mathrm{f}}}{\dot{I}_{\mathrm{D}}}=Z_{\mathrm{DM(1)}}+\dfrac{\dot{I}_{\mathrm{f}}}{\dot{I}_{\mathrm{D}}}R_{\mathrm{f}}= \\ \qquad Z_{\mathrm{DM(1)}}+\dfrac{\dot{I}_{\mathrm{f.A}}}{\dot{I}_{\mathrm{D.A}}+3k_{\mathrm{DM}}\dot{I}_{\mathrm{D(0)}}}R_{\mathrm{f}} \end{cases} \tag{3}$$

where $\dot{U}_{\mathrm{D}}$ is the measured voltage at QF3; $\dot{I}_{\mathrm{D(0)}}$ is the zero-sequence current at QF3; $\dot{I}_{\mathrm{D.A}}$ is the fault-phase current at QF3; $Z_{\mathrm{DM(1)}}$ is the positive-sequence impedance of line MD; and k_{DM} is the zero-sequence current compensation parameter. Since the fault-point current $\dot{I}_{\mathrm{f.A}}$ consists of short-circuit currents at QF2 and QF3, the additional impedances Z_{ad1} and Z_{ad2} at QF2 and QF3 are:

$$\begin{cases} Z_{\mathrm{ad1}}=\dfrac{\dot{I}_{\mathrm{D.A}}+\dot{I}_{\mathrm{N.A}}}{\dot{I}_{\mathrm{N.A}}+3k_{\mathrm{MN}}\dot{I}_{\mathrm{N(0)}}}R_{\mathrm{f}} \\ Z_{\mathrm{ad2}}=\dfrac{\dot{I}_{\mathrm{D.A}}+\dot{I}_{\mathrm{N.A}}}{\dot{I}_{\mathrm{D.A}}+3k_{\mathrm{DM}}\dot{I}_{\mathrm{D(0)}}}R_{\mathrm{f}} \end{cases} \tag{4}$$

Equation (4) shows that if the gaps are not broken down, the neutral points are ungrounded and $\dot{I}_{\mathrm{N(0)}}=\dot{I}_{\mathrm{D(0)}}=0$. DPS-II at QF2 and QF3 does not operate. If the gaps are broken down, $\dot{I}_{\mathrm{N(0)}}$ and $\dot{I}_{\mathrm{D(0)}}$ cease to be 0. The additional impedance and measured impedance are associated with the zero-sequence current at the protection location, fault-phase current, and transition resistance. Therefore, a thorough analysis of the failure mechanism of DPS-II on the DG side is required.

C. Analysis of Failure Mechanism of DPS-II on the DG Side

The fault-phase current ratio at QF2 and QF3 is defined as $x=\dot{I}_{\mathrm{D.A}}/\dot{I}_{\mathrm{N.A}}$. Taking Z_{N} as an example, there is:

$$Z_{\mathrm{N}}=Z_{\mathrm{MN}(1)}+\frac{\dot{I}_{\mathrm{D.A}}+\dot{I}_{\mathrm{N.A}}}{\dot{I}_{\mathrm{N.A}}+3k_{\mathrm{MN}}\dot{I}_{\mathrm{N}(0)}}R_{\mathrm{f}}=Z_{\mathrm{MN}(1)}+\frac{x+1}{1+\frac{2\dot{I}_{\mathrm{N}(0)}}{\dot{I}_{\mathrm{N.A}}}}R_{\mathrm{f}} \tag{5}$$

In (5), the measured impedance at QF2, Z_{N} is related to x and $\dot{I}_{\mathrm{N}(0)}/\dot{I}_{\mathrm{N.A}}$. The examination of the fault-phase sequence currents is crucial. After the neutral points are grounded, the composite sequence network diagram is depicted in Fig. 5, where Z_{W} is the 10 kV line impedance; Z_{T} is the transformer impedance; Z_{L} is the load impedance; and subscripts (1), (2), and (0) denote the positive-sequence, negative-sequence, and zero-sequence components, respectively.

Figure 5 depicts the DGs as current sources employing positive-sequence control strategies. The grounded neutral points trigger the generation of zero-sequence currents at the high-voltage sides of the 110/10 kV transformers. Thus, $\dot{I}_{\mathrm{D.A}}$ and $\dot{I}_{\mathrm{N.A}}$ can be represented as:

$$\begin{cases}\dot{I}_{\mathrm{D.A}}=\dot{I}_{\mathrm{D}(1)}+\dot{I}_{\mathrm{D}(2)}+\dot{I}_{\mathrm{D}(0)}\\ \dot{I}_{\mathrm{N.A}}=\dot{I}_{\mathrm{N}(1)}+\dot{I}_{\mathrm{N}(2)}+\dot{I}_{\mathrm{N}(0)}\end{cases} \tag{6}$$

If the effects of $\dot{I}_{\mathrm{DG1}}$ to $\dot{I}_{\mathrm{D.A}}$ and $\dot{I}_{\mathrm{DG2}}$ to $\dot{I}_{\mathrm{N.A}}$ are neglected, the sequence currents of the fault phase at QF2 and QF3 can be expressed as (7) and (8), respectively.

$$\begin{cases}Z_1=\dfrac{Z_{\mathrm{L2}(1)}}{Z_{\mathrm{L2}(1)}+\left[Z_{\mathrm{W2}(1)}+Z_{\mathrm{T2}(1)}+Z_{\mathrm{DM}(1)}+(Z_{\mathrm{MN}(1)}+Z_{\mathrm{W1}(1)}+Z_{\mathrm{T1}(1)}+Z_{\mathrm{L1}(1)})//(Z_{\Sigma(2)}+Z_{\Sigma(0)})\right]}\\ Z_2=Z_1\times\dfrac{Z_{\mathrm{T1}(0)}+Z_{\mathrm{MN}(0)}}{Z_{\mathrm{T1}(0)}+Z_{\mathrm{T2}(0)}+Z_{\mathrm{DM}(0)}+Z_{\mathrm{MN}(0)}}\\ Z_3=Z_2\times\dfrac{Z_{\mathrm{T1}(2)}+Z_{\mathrm{W1}(2)}+Z_{\mathrm{L1}(2)}+Z_{\mathrm{MN}(2)}}{Z_{\mathrm{T1}(2)}+Z_{\mathrm{W1}(2)}+Z_{\mathrm{L1}(2)}+Z_{\mathrm{MN}(2)}+Z_{\mathrm{T2}(2)}+Z_{\mathrm{W2}(2)}+Z_{\mathrm{L2}(2)}+Z_{\mathrm{DM}(2)}}\\ \dot{I}_{\mathrm{D}(1)}=\dot{I}_{\mathrm{DG2}(1)}Z_1\\ \dot{I}_{\mathrm{D}(0)}=\dot{I}_{\mathrm{DG2}(1)}Z_2\\ \dot{I}_{\mathrm{D}(2)}=\dot{I}_{\mathrm{DG2}(1)}Z_3\end{cases} \tag{7}$$

$$\begin{cases}Z_4=\dfrac{Z_{\mathrm{L1}(1)}}{Z_{\mathrm{L1}(1)}+\left[Z_{\mathrm{W1}(1)}+Z_{\mathrm{T1}(1)}+Z_{\mathrm{MN}(1)}+(Z_{\mathrm{DM}(1)}+Z_{\mathrm{W2}(1)}+Z_{\mathrm{T2}(1)}+Z_{\mathrm{L2}(1)})//(Z_{\Sigma(2)}+Z_{\Sigma(0)})\right]}\\ Z_5=Z_4\times\dfrac{Z_{\mathrm{T2}(0)}+Z_{\mathrm{DM}(0)}}{Z_{\mathrm{T1}(0)}+Z_{\mathrm{T2}(0)}+Z_{\mathrm{DM}(0)}+Z_{\mathrm{MN}(0)}}\\ Z_6=Z_5\times\dfrac{Z_{\mathrm{T2}(2)}+Z_{\mathrm{W2}(2)}+Z_{\mathrm{L2}(2)}+Z_{\mathrm{DM}(2)}}{Z_{\mathrm{T1}(2)}+Z_{\mathrm{W1}(2)}+Z_{\mathrm{L1}(2)}+Z_{\mathrm{MN}(2)}+Z_{\mathrm{T2}(2)}+Z_{\mathrm{W2}(2)}+Z_{\mathrm{L2}(2)}+Z_{\mathrm{DM}(2)}}\\ \dot{I}_{\mathrm{N}(1)}=\dot{I}_{\mathrm{DG1}(1)}Z_4\\ \dot{I}_{\mathrm{N}(0)}=\dot{I}_{\mathrm{DG1}(1)}Z_5\\ \dot{I}_{\mathrm{N}(2)}=\dot{I}_{\mathrm{DG1}(1)}Z_6\end{cases} \tag{8}$$

$$\begin{cases}Z_{\Sigma(2)}=(Z_{\mathrm{MN}(2)}+Z_{\mathrm{W1}(2)}+Z_{\mathrm{T1}(2)}+Z_{\mathrm{L1}(2)})//(Z_{\mathrm{DM}(2)}+Z_{\mathrm{W2}(2)}+Z_{\mathrm{T2}(2)}+Z_{\mathrm{L2}(2)})\\ Z_{\Sigma(0)}=\left[Z_{\mathrm{T1}(0)}+Z_{\mathrm{MN}(0)}//(Z_{\mathrm{T2}(0)}+Z_{\mathrm{DM}(0)})\right]+3R_{\mathrm{f}}\end{cases} \tag{9}$$

The comprehensive negative-sequence and zero-sequence impedances of the system are shown in (9). Concurrently, x is expressed as:

$$x=\frac{\dot{I}_{\mathrm{D.A}}}{\dot{I}_{\mathrm{N.A}}}=\frac{\dot{I}_{\mathrm{D}(1)}+\dot{I}_{\mathrm{D}(2)}+\dot{I}_{\mathrm{D}(0)}}{\dot{I}_{\mathrm{N}(1)}+\dot{I}_{\mathrm{N}(2)}+\dot{I}_{\mathrm{N}(0)}}=\frac{\dot{I}_{\mathrm{DG2}(1)}}{\dot{I}_{\mathrm{DG1}(1)}}\times\frac{Z_1+Z_2+Z_3}{Z_4+Z_5+Z_6} \tag{10}$$

where $\dot{I}_{\mathrm{DG1}(1)}$ and $\dot{I}_{\mathrm{DG2}(1)}$ are the positive short-circuit currents output by DG1 and DG2, respectively; P_{DG1} and P_{DG2} are the rated capacities of DG1 and DG2, respectively. Considering that the fault current characteristics of DG1 and DG2 are identical, equation (10) can be transformed into (11), as:

$$x=\frac{m\dot{I}_{\mathrm{DG2.n}}}{m\dot{I}_{\mathrm{DG1.n}}}\times\frac{Z_1+Z_2+Z_3}{Z_4+Z_5+Z_6}=\frac{P_{\mathrm{DG2}}/\dot{U}_{\mathrm{DG2.n}}}{P_{\mathrm{DG1}}/\dot{U}_{\mathrm{DG1.n}}}\times\frac{Z_1+Z_2+Z_3}{Z_4+Z_5+Z_6} \tag{11}$$

where $\dot{I}_{\mathrm{DG1.n}}$ and $\dot{I}_{\mathrm{DG2.n}}$ are the DGs' rated operation currents; $\dot{U}_{\mathrm{DG1.n}}$ and $\dot{U}_{\mathrm{DG2.n}}$ are the rated operating voltages of the DGs; and m is the maximum short-circuit current parameter of the DGs.

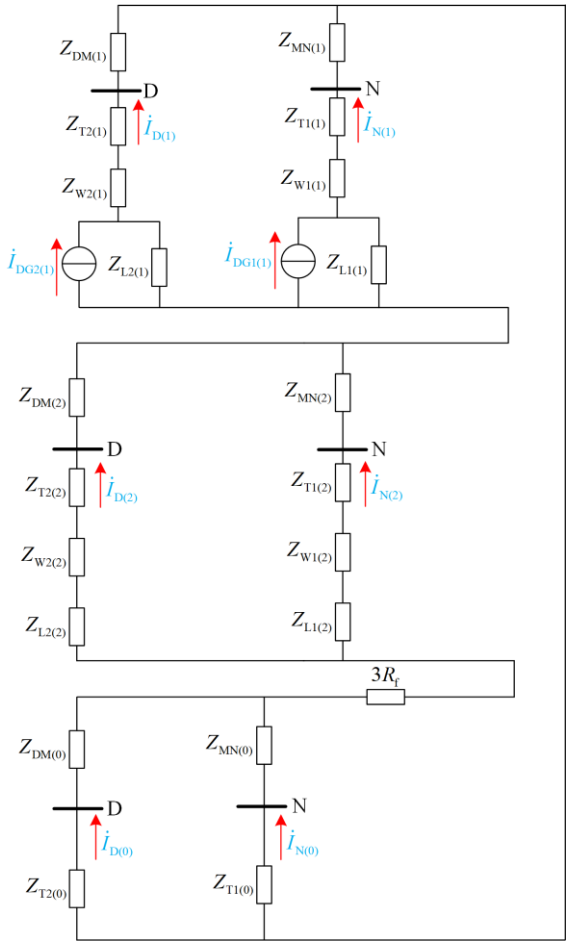

Fig. 5. The composite sequence network diagram after a gap breakdown issue.

Since the fault location is at the main power source side, the voltage drops and states of the DGs can be considered to be consistent. Thus, the DGs are considered to produce the maximum short-circuit currents (if the DGs are in different states, $\dot{I}_{\mathrm{DG1.n}}$ and $\dot{I}_{\mathrm{DG2.n}}$ can also be verified to be associated with P_{DG1} and P_{DG2}, respectively, due to their identical fault characteristics). Then, there is:

$$\dot{U}_{\mathrm{DG1}}=\dot{U}_{\mathrm{DG2}} \tag{12}$$

By combining (10) and (12), equation (10) is simplified as:

$$x=\frac{P_{\mathrm{DG2}}}{P_{\mathrm{DG1}}}\times\frac{Z_1+Z_2+Z_3}{Z_4+Z_5+Z_6} \tag{13}$$

where $(Z_1+Z_2+Z_3)/(Z_4+Z_5+Z_6)$ are commonly represented as the line impedances Z_{W}, transformer impedances Z_{T}; and load impedances Z_{L} at the downstream of QF2 and QF3. Usually, they are complex numbers. The angle difference between $\dot{I}_{\mathrm{D.A}}$ and $\dot{I}_{\mathrm{N.A}}$ for the case $Z_{\mathrm{W1}}=Z_{\mathrm{W2}}$ and $Z_{\mathrm{T1}}=Z_{\mathrm{T2}}$ is shown in Fig. 6. P_{L1} and P_{L2} are the loads at downstream of QF2 and QF3. R_{f} is set to 0–100 Ω, and the downstream impedances of QF2 and QF3 are identical (as expected for Z_{L1} and Z_{L2}). In Fig. 6, when P_{L1} and P_{L2} change, the angle difference between $\dot{I}_{\mathrm{D.A}}$ and $\dot{I}_{\mathrm{N.A}}$ cannot be ignored, which could lead to errors between $\arg(\dot{I}_{\mathrm{f}})$ and $\arg(\dot{I}_{\mathrm{N}})$. For $P_{\mathrm{L2}}>P_{\mathrm{L1}}$, $\arg(\dot{I}_{\mathrm{f}}/\dot{I}_{\mathrm{N}})<0$ and the additional impedance is capacitive, whereas for $P_{\mathrm{L1}}>P_{\mathrm{L2}}$, $\arg(\dot{I}_{\mathrm{f}}/\dot{I}_{\mathrm{N}})>0$ and the additional impedance is inductive. Then, the DPS performance is substantially affected by $\arg(\dot{I}_{\mathrm{f}}/\dot{I}_{\mathrm{N}})$.

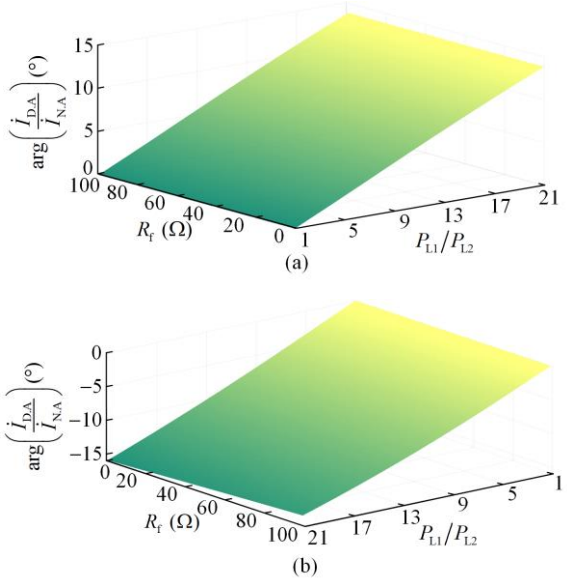

Fig. 6. Phase angle difference between $\dot{I}_{\mathrm{D.A}}$ and $\dot{I}_{\mathrm{N.A}}$. (a) $P_{\mathrm{L1}}>P_{\mathrm{L2}}$. (b) $P_{\mathrm{L2}}>P_{\mathrm{L1}}$.

Notably, Z_{N} is also subjected to $\dot{I}_{\mathrm{D.A}}/\dot{I}_{\mathrm{N.A}}$ in (5), and can be written as:

$$\frac{\dot{I}_{\mathrm{N(0)}}}{\dot{I}_{\mathrm{N.A}}}=\frac{\dot{I}_{\mathrm{N(0)}}}{\dot{I}_{\mathrm{N(1)}}+\dot{I}_{\mathrm{N(2)}}+\dot{I}_{\mathrm{N(0)}}}=\frac{1}{1+\frac{\dot{I}_{\mathrm{N(1)}}}{\dot{I}_{\mathrm{N(0)}}}+\frac{\dot{I}_{\mathrm{N(2)}}}{\dot{I}_{\mathrm{N(0)}}}} \tag{14}$$

According to (8), $\dot{I}_{\mathrm{N(0)}}/\dot{I}_{\mathrm{N(1)}}$ and $\dot{I}_{\mathrm{N(0)}}/\dot{I}_{\mathrm{N(2)}}$ are specified in (15).

$$\begin{cases} \dfrac{\dot{I}_{\mathrm{N}(1)}}{\dot{I}_{\mathrm{N}(0)}} = \dfrac{Z_4}{Z_5} = \dfrac{Z_{\mathrm{T1}(0)} + Z_{\mathrm{T2}(0)} + Z_{\mathrm{DM}(0)} + Z_{\mathrm{MN}(0)}}{Z_{\mathrm{T2}(0)} + Z_{\mathrm{DM}(0)}} \\ \dfrac{\dot{I}_{\mathrm{N}(2)}}{\dot{I}_{\mathrm{N}(0)}} = \dfrac{Z_5}{Z_6} = \dfrac{Z_{\mathrm{T2}(2)} + Z_{\mathrm{W2}(2)} + Z_{\mathrm{L2}(2)} + Z_{\mathrm{DM}(2)}}{Z_{\mathrm{T1}(2)} + Z_{\mathrm{W1}(2)} + Z_{\mathrm{L1}(2)} + Z_{\mathrm{MN}(2)} + Z_{\mathrm{T2}(2)} + Z_{\mathrm{W2}(2)} + Z_{\mathrm{L2}(2)} + Z_{\mathrm{DM}(2)}} \end{cases} \tag{15}$$

Typically, the 110 kV line impedance is small, with $\{Z_{\mathrm{W}}, Z_{\mathrm{L}}, Z_{\mathrm{T}}\} \gg \{Z_{\mathrm{DM}}, Z_{\mathrm{MN}}\}$ and $Z_{\mathrm{L}} \gg \{Z_{\mathrm{W}}, Z_{\mathrm{T}}\}$. Then, equation (15) is transformed into:

$$\begin{cases} \dfrac{\dot{I}_{\mathrm{N}(1)}}{\dot{I}_{\mathrm{N}(0)}} \approx 2 \\ \dfrac{\dot{I}_{\mathrm{N}(2)}}{\dot{I}_{\mathrm{N}(0)}} \approx \dfrac{Z_{\mathrm{L2}}}{Z_{\mathrm{L1}} + Z_{\mathrm{L2}}} \end{cases} \tag{16}$$

Assuming the loads are mostly resistive, $y = Z_{\mathrm{L2}}/(Z_{\mathrm{L1}} + Z_{\mathrm{L2}})$ can be defined as a constant. Substituting (13) and (16) into (5) yields:

$$\begin{aligned} Z_{\mathrm{N}} = Z_{\mathrm{MN}(1)} + \frac{3+y}{5+y} \times (x+1) R_{\mathrm{f}} = \\ \mathrm{Re}(Z_{\mathrm{MN}(1)}) + \frac{3+y}{5+y} R_{\mathrm{f}} \cdot [\mathrm{Re}(x)+1] + \\ \mathrm{Im}(Z_{\mathrm{MN}(1)}) + \frac{3+y}{5+y} R_{\mathrm{f}} \times \mathrm{Im}(x) \end{aligned} \tag{17}$$

Equation (17) illustrates that Z_{N} is associated with $P_{\mathrm{DG2}}/P_{\mathrm{DG1}}$, y, R_{f}, and the fault locations. With the increase in $P_{\mathrm{DG2}}/P_{\mathrm{DG1}}$ and R_{f}, the real and imaginary parts of Z_{N} are simultaneously enlarged. To ensure the reliable action of QF2, Z_{N} should satisfy the action criterion of amplitude comparison in the directional impedance relay [22]:

$$\left| Z_{\mathrm{N}} - \frac{1}{2} Z_{\mathrm{set.N}}^{\mathrm{II}} \right| \leqslant \left| \frac{1}{2} Z_{\mathrm{set.N}}^{\mathrm{II}} \right| \tag{18}$$

where $|\cdot|$ represents the modulus value and $Z_{\mathrm{set.N}}^{\mathrm{II}}$ is the setting value of DPS-II at QF2. The value of $\left|Z_{\mathrm{set.N}}^{\mathrm{II}}\right|$ depends on the 220/110 kV transformer impedance on the reverse side of QF1. When the real part of Z_{N} is raised, $\left| Z_{\mathrm{N}} - \frac{1}{2} Z_{\mathrm{set.N}}^{\mathrm{II}} \right|$ is augmented. If (18) is unsatisfied, QF2 will not trip. The same analysis method is also suitable for the measured impedance Z_{D}.

Next, based on (17) and (18), the relationship between $\left| Z_{\mathrm{N}} - \frac{1}{2} Z_{\mathrm{set.N}}^{\mathrm{II}} \right|$ and $\left| \frac{1}{2} Z_{\mathrm{set.N}}^{\mathrm{II}} \right|$ is displayed in Fig. 7. For convenient calculation, $Z_{\mathrm{L1}(2)} = Z_{\mathrm{L2}(2)}$ and $y = 1/2$ are pre-set. For $R_{\mathrm{f}} = 0 - 10\ \Omega$, equation (18) is likely to be satisfied for a large value of $P_{\mathrm{DG2}}/P_{\mathrm{DG1}}$. However, for $R_{\mathrm{f}} = 20 - 100\ \Omega$, equation (18) is theoretically not satisfied with the increase in $P_{\mathrm{DG2}}/P_{\mathrm{DG1}}$, preventing the tripping of QF2.

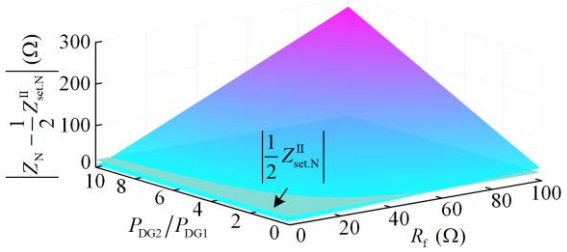

Fig. 7. Relationship between $\left| Z_{\mathrm{N}} - \frac{1}{2} Z_{\mathrm{set.N}}^{\mathrm{II}} \right|$ and $\left| \frac{1}{2} Z_{\mathrm{set.N}}^{\mathrm{II}} \right|$.

Next, an SPGF at 2.0 s is considered to observe $\left| Z_{\mathrm{N}} - \frac{1}{2} Z_{\mathrm{set.N}}^{\mathrm{II}} \right|$. QF1 trips at 2.1 s, and the fault scenarios are assumed as follows. The local loads at downstream of QF2 and QF3 are both 2 MW; R_{f} is set as 20 Ω and 100 Ω, respectively; $P_{\mathrm{DG1}} = 2$ MW and $P_{\mathrm{DG2}} = 6$ MW, 8 MW, 10 MW, and 12 MW. Moreover, "1" implies that QF2 correctly trips, and "0" implies that QF2 does not trip. In Fig. 8(a), $\left| Z_{\mathrm{N}} - \frac{1}{2} Z_{\mathrm{set.N}}^{\mathrm{II}} \right| > \left| \frac{1}{2} Z_{\mathrm{set.N}}^{\mathrm{II}} \right|$ is satisfied for $R_{\mathrm{f}} = 20 - 100\ \Omega$. Take the value of $\left| Z_{\mathrm{N}} - \frac{1}{2} Z_{\mathrm{set.N}}^{\mathrm{II}} \right|$ at 2.135 s (nearly one cycle after gap breakdown) as an example. For $R_{\mathrm{f}} = 20\ \Omega$, with the increase in P_{DG2}, $\left| Z_{\mathrm{N}} - \frac{1}{2} Z_{\mathrm{set.N}}^{\mathrm{II}} \right|$ is 35.28 Ω, 36.67 Ω, 37.63 Ω, and 38.23 Ω. For $R_{\mathrm{f}} = 100\ \Omega$, with the increase in P_{DG2}, $\left| Z_{\mathrm{N}} - \frac{1}{2} Z_{\mathrm{set.N}}^{\mathrm{II}} \right|$ is 113.09 Ω, 121.40 Ω, 127.47 Ω, and 132.14 Ω. The value of $\left| Z_{\mathrm{N}} - \frac{1}{2} Z_{\mathrm{set.N}}^{\mathrm{II}} \right|$ increases with P_{DG2} in the gap-grounded system. In Figs. 8(b) and (c), because the action criterion is never satisfied, QF2 does not trip. Thus, the action performance of the DPS in the gap-grounded system is affected by the gap breakdown and fault transition resistance R_{f}.

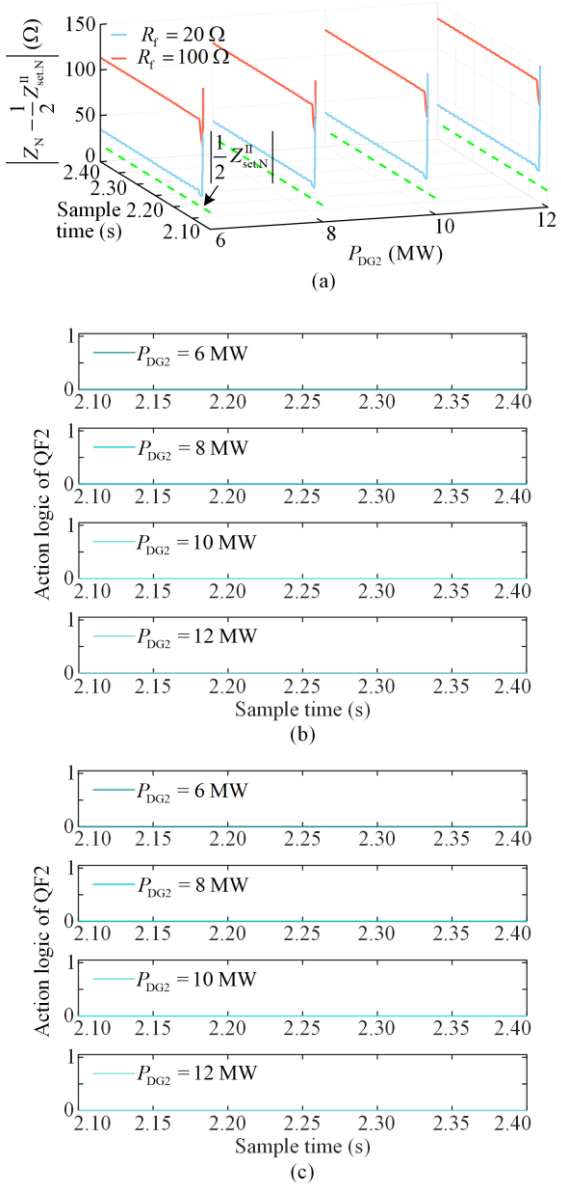

Fig. 8. $\left|Z_N - \frac{1}{2}Z^{II}_{set.N}\right|$ and action logic of QF2. (a) $\left|Z_N - \frac{1}{2}Z^{II}_{set.N}\right|$ and $\left|\frac{1}{2}Z^{II}_{set.N}\right|$. (b) $R_f = 20\,\Omega$. (c) $R_f = 100\,\Omega$.

The results of the above analysis can be briefly summarized as follows. For a multiple-DG network, the DG capacity affects the measured impedance and protection action performance. In addition, if the air gap is broken down, a zero-sequence network is created and the action criterion of DPS-II may not be satisfied.

III. Research on DPS in the Gap-Grounded System

The analysis in Section II reveals that the measured impedance consists of the real short-circuit impedance and additional impedance [32]. The real short-circuit impedance serves as an indicator of the fault location, remaining relatively stable for a known fault. Nevertheless, the additional impedance is affected by fault currents and fault transition resistances. To eliminate the additional impedance, an improved DPS is proposed based on the real short-circuit impedance in T-type networks with a single DG and multiple DGs.

A. DPS for the Forward Fault

Given that the influencing factors in T-type networks with a single DG and multiple DGs are different, DPS can be categorized into two parts.

1) T-type Network with Single DG

When the single DG is connected to the T-type network and an SPGF occurs in the forward region of QF2, the relationship between the impedance phasors in the directional impedance relay is shown in Fig. 9.

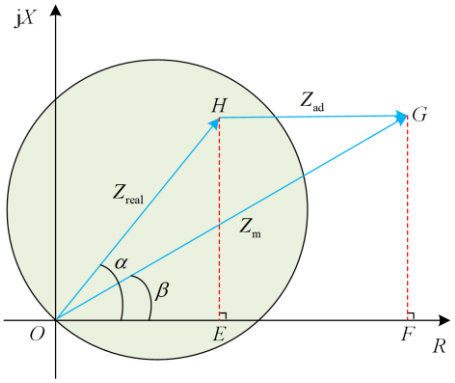

Fig. 9. Impedance relationship for a forward fault in the T-type network with a single DG.

For the protection at bus N, the measured impedance Z_m, real short-circuit impedance Z_{real}, and additional impedance Z_{ad} are written as:

$$\begin{cases} Z_m = Z_{real} + Z_{ad} \\ Z_{real} = Z_{MN(1)} \\ Z_{ad} = \dfrac{\dot{I}_f}{\dot{I}_N} R_f = \dfrac{\dot{I}_{f.A}}{\dot{I}_{N.A} + 3k_{MN}\dot{I}_{N(0)}} R_f \end{cases} \tag{19}$$

where α is the line impedance angle; and β is the measured impedance angle. After QF1 trips, $\left|\dot{I}_{f.A}\right| = \left|\dot{I}_{N.A}\right|$ and $\arg(\dot{I}_{f.A}) = \arg(\dot{I}_{N.A}) = \arg(\dot{I}_{N(0)})$, as only one branch is connected with the DG. As a result, Z_{ad} is fully resistive, indicating Z_{ad} is parallel to the R-axis and the additional impedance angle is $0°$. From (19) and Fig. 9, the value of Z_m mainly depends on R_f. With an increase in R_f, Z_m increases to beyond the action area of the impedance circle. During this process, the resistance part of Z_m is altered, while its reactance part remains constant. This implies that $\mathrm{Im}(Z_m) = \mathrm{Im}(Z_{real})$ for all R_f. When $\mathrm{Im}(Z_m)$ is determined, the real short-circuit impedance Z_{real} can be obtained.

Two right triangles ΔOEH and ΔOFG are established in the impedance circle to solve $\mathrm{Im}(Z_{\mathrm{real}})$. In ΔOEH and ΔOFG, there $|EH|=|GF|$. Then, $\mathrm{Im}(Z_{\mathrm{real}})$ is calculated as:

$$\mathrm{Im}(Z_{\mathrm{m}})=\mathrm{Im}(Z_{\mathrm{real}})=|Z_{\mathrm{m}}|\times\sin\beta \tag{20}$$

where both Z_{m} and β can be obtained at the local protection. Assuming that the unit line impedance of MN is z_{MN}, then Z_{real} can be represented as:

$$\begin{cases} Z_{\mathrm{real}}=z_{\mathrm{MN}}\times\dfrac{\mathrm{Im}(Z_{\mathrm{real}})}{\mathrm{Im}(z_{\mathrm{MN}})}=\dfrac{z_{\mathrm{MN}}}{\mathrm{Im}(z_{\mathrm{MN}})}\times K_{\mathrm{real}}|Z_{\mathrm{m}}| \\ K_{\mathrm{real}}=\sin\beta>0 \end{cases} \tag{21}$$

where $\mathrm{Im}(z_{\mathrm{MN}})$ is the reactance part of z_{MN}; and K_{real} is a distance protection parameter. Based on (21), the effect of R_{f} on Z_{m} can be alleviated in the single-DG network. Moreover, β is an inner angle in the triangle ΔOFG. Thus, $K_{\mathrm{real}}>0$ is theoretically satisfied in a forward fault.

2) T-type Network with Multiple DGs

When the multiple DGs are connected to a T-type network, $\arg(\dot{I}_{\mathrm{f.A}})\neq\arg(\dot{I}_{\mathrm{N.A}})$, due to the angle difference. If this difference cannot be neglected, the value of Z_{real} cannot be solved by (21). Assuming the additional impedance angle $\gamma\in(-\pi/2,\pi/2)$, the impedance relationships with $\gamma\in(-\pi/2,0)$ and $\gamma\in(0,\pi/2)$ are displayed in Fig. 10.

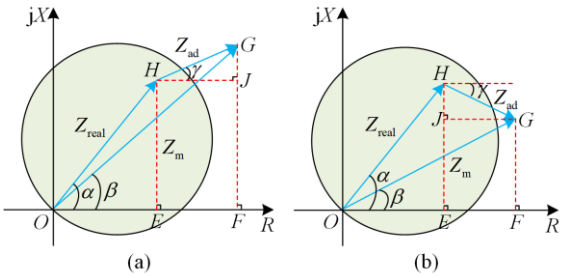

Fig. 10. Impedance relationships for forward faults in a T-type network with multiple DGs. (a) $\gamma\in(0,\pi/2)$. (b) $\gamma\in(-\pi/2,0)$.

Based on the sine theorem in Fig. 10(a), there are:

$$\begin{cases} \angle OHG=180^{\circ}+\gamma-\alpha \\ \angle HGO=\beta-\gamma \\ \dfrac{|Z_{\mathrm{m}}|}{\sin(\angle OHG)}=\dfrac{|Z_{\mathrm{real}}|}{\sin(\angle HGO)} \end{cases} \tag{22}$$

Equation (22) can be transformed into (23) as follows:

$$|Z_{\mathrm{real}}|=|Z_{\mathrm{m}}|\frac{\sin(\beta-\gamma)}{\sin(\alpha-\gamma)} \tag{23}$$

Similarly, equation (24) can be obtained from Fig. 10(b) as:

$$\begin{aligned} |Z_{\mathrm{real}}|&=|Z_{\mathrm{m}}|\frac{\sin(\angle HGO)}{\sin(\angle OHG)}=|Z_{\mathrm{m}}|\frac{\sin(\beta-\gamma)}{\sin(180^{\circ}+\gamma-\alpha)}= \\ &|Z_{\mathrm{m}}|\frac{\sin(\beta-\gamma)}{\sin(\alpha-\gamma)} \end{aligned} \tag{24}$$

Equation (24) contains the same expression for $|Z_{\mathrm{real}}|$ as in (23). To sum up, $|Z_{\mathrm{real}}|$ for a forward fault at QF2 be denoted as follows:

$$\begin{cases} |Z_{\mathrm{real}}|=|Z_{\mathrm{m}}|\times\dfrac{\sin(\beta-\gamma)}{\sin(\alpha-\gamma)}=K'_{\mathrm{real}}|Z_{\mathrm{m}}| \\ K'_{\mathrm{real}}=\dfrac{\sin(\beta-\gamma)}{\sin(\alpha-\gamma)}>0 \end{cases} \tag{25}$$

Considering that $\angle OHG$ and $\angle HGO$ are inner angles of the triangles, $K'_{\mathrm{real}}>0$ is always satisfied for the forward faults. Then, Z_{real} is represented as:

$$Z_{\mathrm{real}}=z_{\mathrm{MN}}\times\frac{K'_{\mathrm{real}}|Z_{\mathrm{m}}|}{|z_{\mathrm{MN}}|} \tag{26}$$

In a T-type network with multiple DGs, Z_{real} can be calculated using (26). By substituting Z_{N} in (18) with Z_{real}, there is:

$$\left|Z_{\mathrm{real}}-\frac{1}{2}Z^{\mathrm{II}}_{\mathrm{set.N}}\right|\leqslant\left|\frac{1}{2}Z^{\mathrm{II}}_{\mathrm{set.N}}\right| \tag{27}$$

Thus, equation (27) can be considered a new protection action criterion for the forward faults. However, $\mathrm{Im}(Z_{\mathrm{ad}})$ is capacitive, and transient overreach may occur. Thus, DPS-I at QF2 will incorrectly operate.

In Fig. 11, $|Z^{\mathrm{I}}_{\mathrm{set.N}}|$ is the setting value of DPS-I at QF2. For $\gamma\in(-\pi/2,0)$, DPS-I at QF2 possibly incorrectly operates due to transient overreach. Further, the maximum γ corresponds to Z_{ad} being tangent to the impedance circle, and the minimum γ is $-\pi/2$. Thus, the additional impedance angle meets the condition $\gamma\in(-\pi/2,\alpha-\pi/2)$. Given that γ is influenced by the downstream impedances of QF2 and QF3, DPS-I at QF2 may incorrectly operate before DPS-II operates.

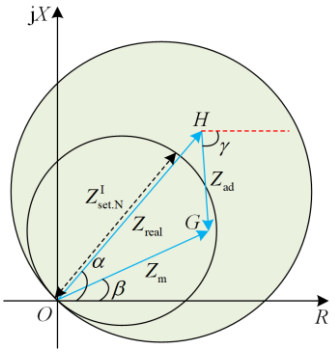

Fig. 11. Impedance relationship for transient overreach.

However, Z_{real} in Fig. 11 can be solved by (26). Then, there is:

$$|Z_{\text{real}}| \geqslant |Z^{\text{I}}_{\text{set.N}}| \tag{28}$$

Based on (28), overreach issues can be effectively addressed to avoid incorrect operation of DPS-I.

B. DPS for the Reverse Fault

To prevent the protection from incorrectly operating for reverse faults, it is necessary to analyze the protection criterion.

1) T-type Network with Single DG

Assume that an SPGF occurs on the reverse side of bus N and only one branch is connected with the DG in the T-type network after QF1 trips. This implies that no fault current flows through QF2, and the fault-phase current at the protection location is $|\dot{I}_{\text{N.A}}| = 0$. Therefore, the reverse fault in the T-type network with a single DG can be recognized using $\dot{I}_{\text{N.A}}$.

2) T-type Network with Multiple DGs

In the T-type network with multiple DGs, all branches are connected with the DGs and $|\dot{I}_{\text{N.A}}| \neq 0$. The phasor relationship in the impedance circle when QF2 incorrectly operates under a reverse fault is displayed in Fig. 12.

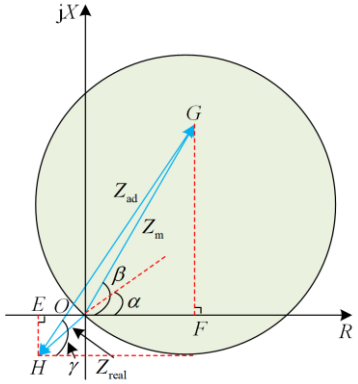

Fig. 12. Impedance relationship for reverse faults in a T-type network with multiple DGs.

In Fig. 12, there are:

$$\begin{cases} \angle OHG = \gamma - \alpha \\ \angle HGO = \beta - \gamma \end{cases} \tag{29}$$

Then, K'_{real} can be further derived as:

$$K'_{\text{real}} = \frac{\sin(\beta-\gamma)}{\sin(\alpha-\gamma)} = -\frac{\sin(\angle OHG)}{\sin(\angle HGO)} < 0 \tag{30}$$

Similarly, K'_{real} is always satisfied for reverse faults. By combining (25) and (30), the relationship between K'_{real} and fault direction based on the directional impedance circle is derived as:

$$\begin{cases} K'_{\text{real}} > 0, \text{ Forward fault} \\ K'_{\text{real}} < 0, \text{ Reverse fault} \end{cases} \tag{31}$$

Notably, the line impedance angle α and measured impedance angle β can be obtained based on the local information, but the direct solution of the additional impedance angle γ is difficult.

C. Analysis of Additional Impedance Angle

Based on the analysis in Section III.A, $\arg(\dot{I}_{\text{f.A}}) = \arg(\dot{I}_{\text{N.A}})$ is assured for a single-DG network, and the additional impedance angle γ is considered to be 0°. In a multiple-DG network, $\gamma = \arg(\dot{I}_{\text{N.A}} + \dot{I}_{\text{D.A}}) - \arg(\dot{I}_{\text{N.A}} + 3k_{\text{MN}}\dot{I}_{\text{N(0)}})$. However, because no communication channel exists between QF2 and QF3, the direct derivation of γ is difficult to obtain. Then, the local electrical quantities of QF2 need to be inevitably used to express γ. When an SPGF occurs, according to the boundary condition and Fig. 5, there are [33]:

$$\dot{I}_{\text{f.A}} = 3\dot{I}_{\text{f.A(2)}} = 3\dot{I}_{\text{f.A(1)}} = 3\frac{\dot{I}_{\text{N(2)}}}{C_{\text{N(2)}}} = 3\frac{\dot{I}_{\text{N(1)}}}{C_{\text{N(1)}}} \tag{32}$$

where $C_{\text{N(1)}}$ and $C_{\text{N(2)}}$ are the positive and negative-sequence current distribution coefficients, respectively. Considering (8) and Fig. 5, $C_{\text{N(1)}}$ can be represented as:

$$C_{\text{N(1)}} = \frac{\dot{I}_{\text{DG1(1)}} Z_4}{\dot{I}_{\text{DG1(1)}} Z_4 + \dot{I}_{\text{DG2(1)}} Z_1} \tag{33}$$

The traditional schemes [33] and [34] utilize the positive-sequence current distribution factor to represent the fault current to solve the additional impedance angle γ. However, $C_{\text{N(1)}}$ in (33) cannot be calculated using the local electrical quantities and is regarded as a constant. Consequently, $C_{\text{N(2)}}$ is recommended for solving γ, as:

$$C_{\text{N(2)}} = \frac{Z_{\text{T2(2)}} + Z_{\text{W2(2)}} + Z_{\text{L2(2)}} + Z_{\text{DM(2)}}}{Z_{\text{T1(2)}} + Z_{\text{W1(2)}} + Z_{\text{L1(2)}} + Z_{\text{MN(2)}} + Z_{\text{T2(2)}} + Z_{\text{W2(2)}} + Z_{\text{L2(2)}} + Z_{\text{DM(2)}}} \tag{34}$$

Because $Z_{\text{L}} \gg \{Z_{\text{W}}, Z_{\text{T}}, Z_{\text{DM}}, Z_{\text{MN}}\}$, $C_{\text{N(2)}}$ can be rewritten as:

$$C_{\text{N(2)}} \approx \frac{Z_{\text{L2(2)}}}{Z_{\text{L1(2)}} + Z_{\text{L2(2)}}} = y \tag{35}$$

Based on the analysis in Section II, $C_{\text{N(2)}}$ can be considered a constant. Then, γ is transformed into:

$$\gamma = \arg\left(\frac{\dot{I}_{\text{f.A}}}{\dot{I}_{\text{N.A}} + 3k_{\text{MN}}\dot{I}_{\text{N(0)}}}\right) = \arg\left[\frac{3\dot{I}_{\text{N(2)}}}{C_{\text{N(2)}}(\dot{I}_{\text{N.A}} + 3k_{\text{MN}}\dot{I}_{\text{N(0)}})}\right] = \arg\left(\frac{\dot{I}_{\text{N(2)}}}{\dot{I}_{\text{N.A}} + 3k_{\text{MN}}\dot{I}_{\text{N(0)}}}\right) = \arg\left(\dot{I}_{\text{N(2)}}\right) - \arg\left(\dot{I}_{\text{N.A}} + 3k_{\text{MN}}\dot{I}_{\text{N(0)}}\right) \tag{36}$$

In (36), γ can be solved by exploiting the local electrical quantities. Overall, an improved DPS for the power system with gap-grounded transformers can be established, and the corresponding flowchart is depicted in Fig. 13.

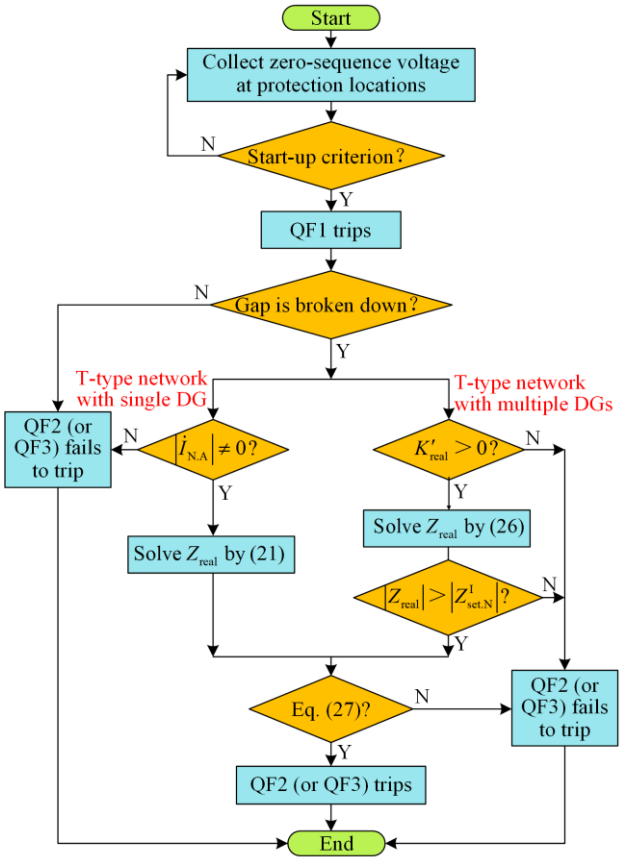

Fig. 13. Flowchart of improved DPS for a system with gap-grounded transformers.

The main steps of Fig. 13 are listed as follows.

Step 1: Collect the zero-sequence voltage at the protection locations. Typically, when an SPGF occurs, the zero-sequence voltage at the bus is more than 15% of the rated phase voltage, which can be used as a start-up criterion for the protection.

Step 2: If the zero-sequence voltage at the bus satisfies the start-up criterion, DPS-I rapidly operates, and QF1 trips after 100 ms. Otherwise, perform step 1.

Step 3: Observe the neutral-point voltage (equal to the zero-sequence voltage at bus N or D) for 15 ms after QF1 trips. If the neutral-point voltage is less than the gap breakdown voltage, QF2 and QF3 do not trip. Otherwise, perform step 4.

Step 4: For the T-type network with a single DG, if the fault-phase current at the protection location is 0, QF2 and QF3 do not trip. Otherwise, Z_{real} can be obtained from (21) and then perform step 6. For a T-type network with multiple DGs, if $K'_{real} < 0$, QF2 and QF3 do not trip. Otherwise, Z_{real} can be obtained from (26) and step 5 is performed.

Step 5: If $|Z_{real}| < |Z^{I}_{set.N}|$, QF2 and QF3 do not operate. Otherwise, perform step 6.

Step 6: If Z_{real} continuously satisfies the action criterion (27) for 300–500 ms, QF2 and QF3 are allowed to trip.

The probability of an SPGF in the distribution network is approximately 60%–80%, while two-phase to ground faults can be attributed to SPGFs. In addition, the neutral-point voltage of an SPGF is much higher than that of a two-phase to ground fault owing to the parallel connection of the composite sequence network [7]. Therefore, the fault analysis and simulations of the two-phase-to-ground faults a omitted in this study.

IV. Simulation Results

To assess the effectiveness of the improved DPS, a simulation platform is constructed using MATLAB @ 2018b and PSCAD/EMTDC-V46 with Windows 11, Intel i7-12700H, 2.70 GHz processor, and 16 GB RAM. The main simulation parameters are shown in Table II. Moreover, all simulation results match the measured impedance and protection action performance at QF2. The simulation results at QF3 can be obtained similarly and are therefore omitted here.

TABLE II
Main Simulation Parameters

Parameter	Value
Length of MN (km)	10
Length of ND (km)	10
Fault phase	A
Positive-sequence impedance of 110 kV line (Ω)	0.13+j0.39
Zero-sequence impedance of 110 kV line (Ω)	0.39+j1.17
110 kV line impedance angle (°)	71.57
System capacity of 220 /110 kV transformer (MVA)	100
System capacity of 110 /10 kV transformer (MVA)	50
Leakage reactance (p.u.)	0.1
Rated capacity of DG (MW)	5-20
Transition resistance (Ω)	0.01-100
Gap breakdown voltage (kV)	72.25
Setting value of DPS-I at QF2 (Ω)	1.04+j3.12
Setting value of DPS-II at QF2 (Ω)	0.73+j36.07
Sampling frequency (Hz)	10 000

Unless otherwise stated, the fault occurs at 2.0 s and QF1 trips at 2.1 s in the simulation. The simulation models for different scenarios are shown in Fig. 14. For a T-type network with a single DG, the DG is connected only at line MN. The neutral points of the 110/10 kV transformers are all grounded by air gaps. Moreover, the neutral points adopt the element "Spark Gap" in the PSCAD. It can effectively suppress the neutral-point

voltage, and the breakdown voltage can be pre-set. The breakdown voltage is usually greater than the rated phase voltage of the transformer ($110/\sqrt{3} \approx 63.5$ kV). Considering extreme cases, this study set the breakdown voltage as 72.25 kV based on Table I.

The proposed scheme aims to eliminate the effect of the additional impedance angle γ on the protection action performance. Hence, γ is analyzed under different SPGF scenarios.

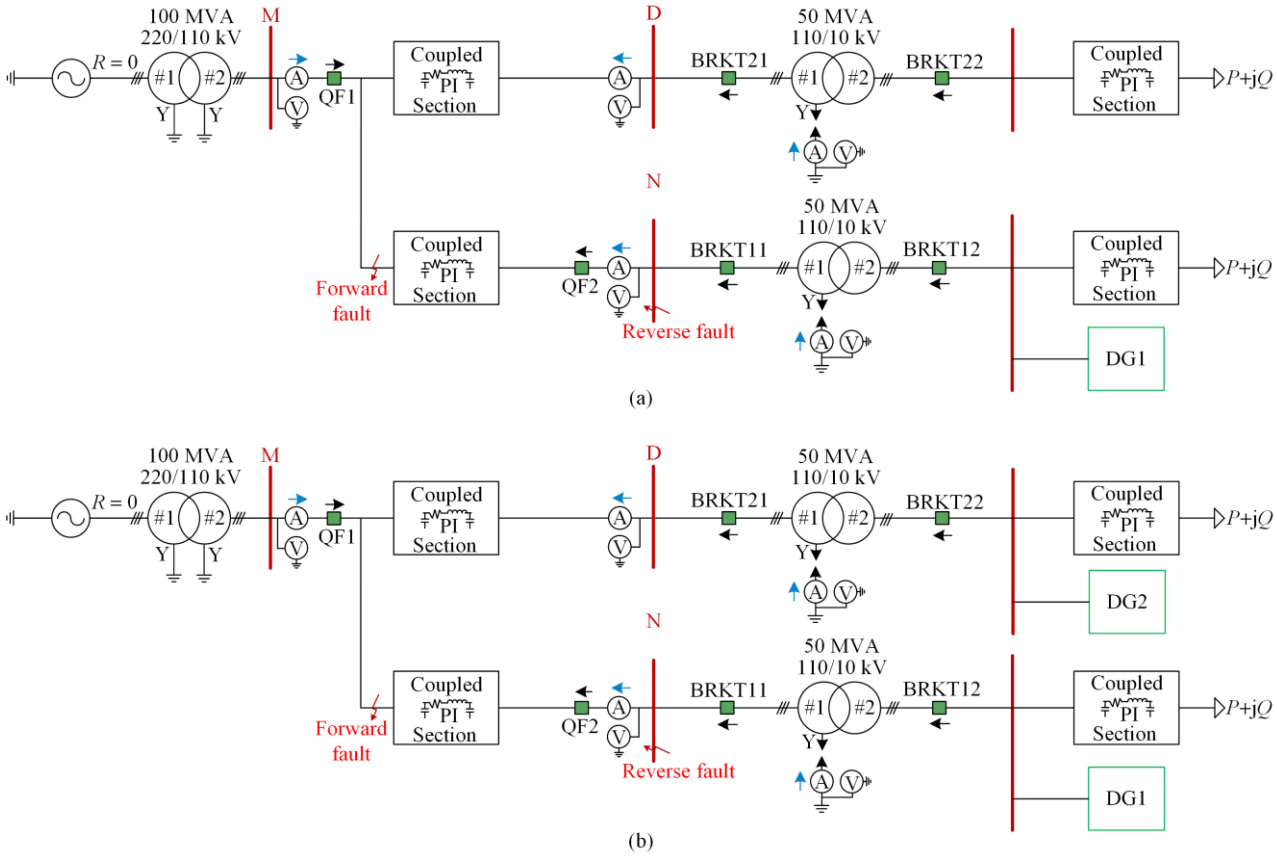

Fig. 14. Simulation models for different scenarios. (a) T-type network with single DG. (b) T-type network with multiple DGs.

In Figs. 15(a)–(c), forward faults are applied with various P_{L1} and P_{L2}. When $P_{L1} = P_{L2}$, γ is approximately 0°, which implies that Z_{ad} is close to being resistive. However, as the relationship between P_{L1} and P_{L2} changes, Z_{ad} varies between inductive and capacitive. In Fig. 15(d), $\gamma \in (\alpha - \pi/2, \pi/2)$ also conforms to the theoretical analysis.

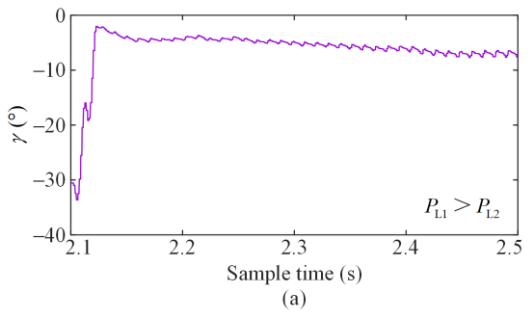

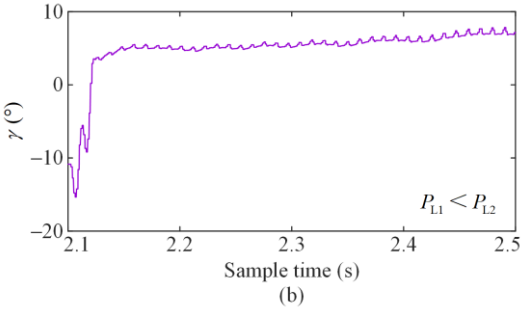

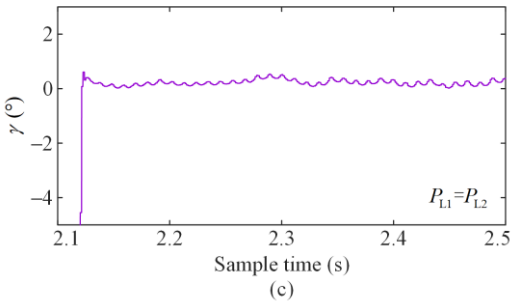

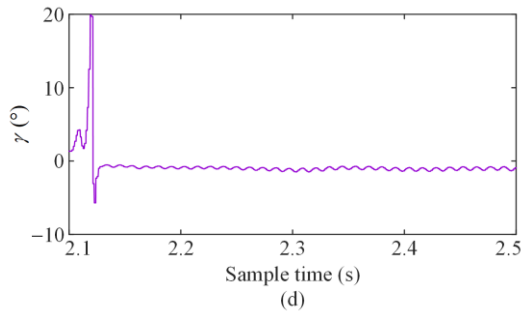

Fig. 15. γ in different fault scenarios. (a) Forward fault 1. (b) Forward fault 2. (c) Forward fault 3. (d) Reverse fault.

A. Validation for a T-type Network with Single DG

First of all, the effectiveness of the improved DPS should be verified.

1) Forward Faults

In the single-DG network, the SPGF occurs at the beginning of the line MD. The local loads P_{L1} and P_{L2} are set as 2 MW, and the DG is connected to the downstream of QF2. The fault distance parameter is defined as:

$$\lambda = \frac{l_{Nf}}{l_{MN}} \times 100\% \tag{37}$$

where l_{Nf} is the length from QF1 to the fault point and l_{MN} is the length of line MN.

Cases 1–3 in Table III are used to validate the effectiveness of the proposed scheme with different fault transition resistances R_f, rated capacities P_{DG}, and fault locations λ.

In Figs. 16–18, $\left|Z_{real}\right|$ is the modulus value of Z_{real} solved by (21) and $\left|Z_{Nf}\right|$ is the modulus value of the line impedance from the fault point to QF2.

TABLE III
SIMULATION PARAMETERS FOR CASES 1–3

Variable	R_f (Ω)	P_{DG} (MW)	λ (%)
Case 1	20, 40, 80, 100	10	100
Case 2	100	12, 16, 18, 20	100
Case 3	50	10	100, 95, 90, 85

As shown in Figs. 16–18, the values of $\left|Z_{real}\right|$ are close to those of $\left|Z_{Nf}\right|$ for all scenarios when utilizing (21), which validates the effectiveness of the proposed scheme. In addition, $\left|Z_{real} - \frac{1}{2}Z^{II}_{set.N}\right| \leqslant \left|\frac{1}{2}Z^{II}_{set.N}\right|$ (18.035 Ω) is satisfied by replacing Z_N with Z_{real}. The action logic of QF2 is clearly maintained at "1" after 2.135 s, and DPS-II can reliably trip. In Fig. 19, the distance protection parameter $K_{real} > 0$ in all cases indicates that the faults are in the forward region of QF2, which verifies the theoretical analysis. Thus, the reliability of the protection action is realized in the single-DG network for forward faults.

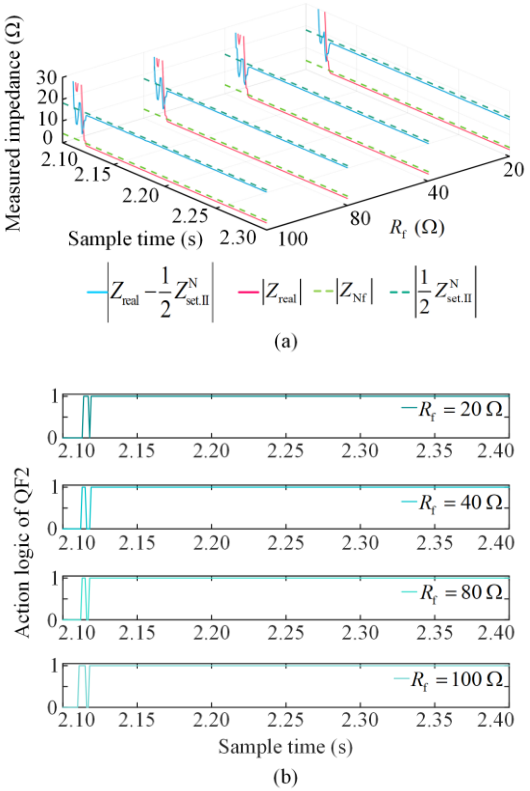

Fig. 16. Case 1: action performance of QF2 with different R_f. (a) Measured impedances. (b) Action logic of QF2.

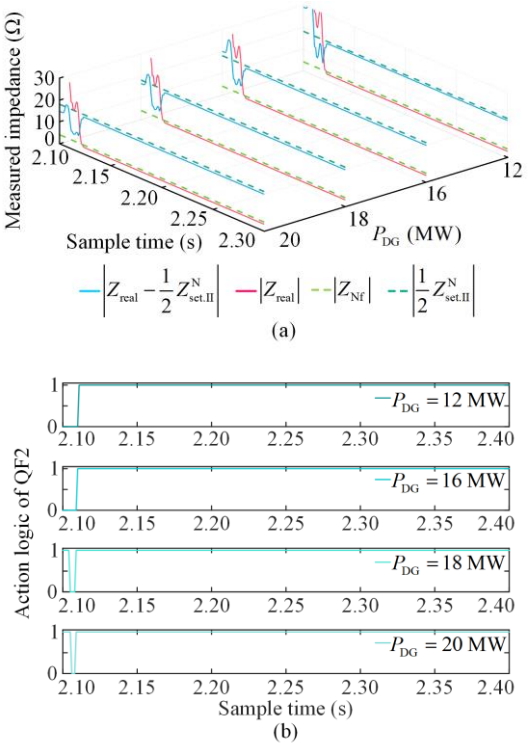

Fig. 17. Case 2: Action performance of QF2 with different P_{DG}.

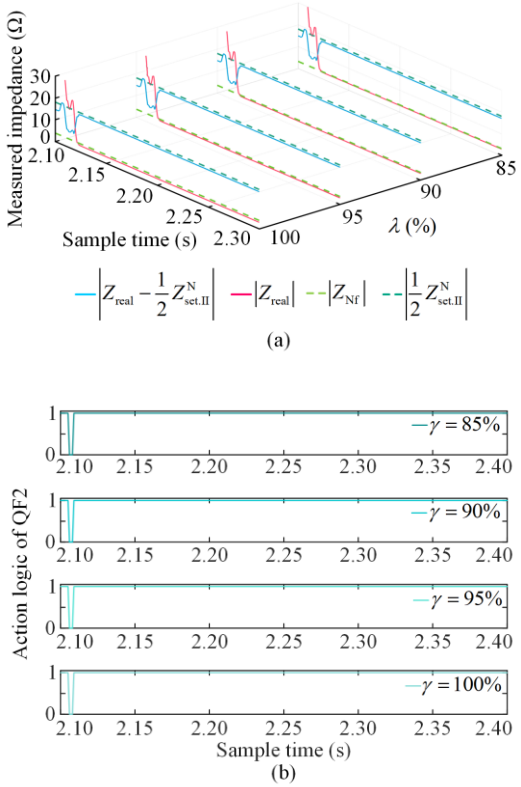

Fig. 18. Case 3: Action performance of QF2 with different λ.

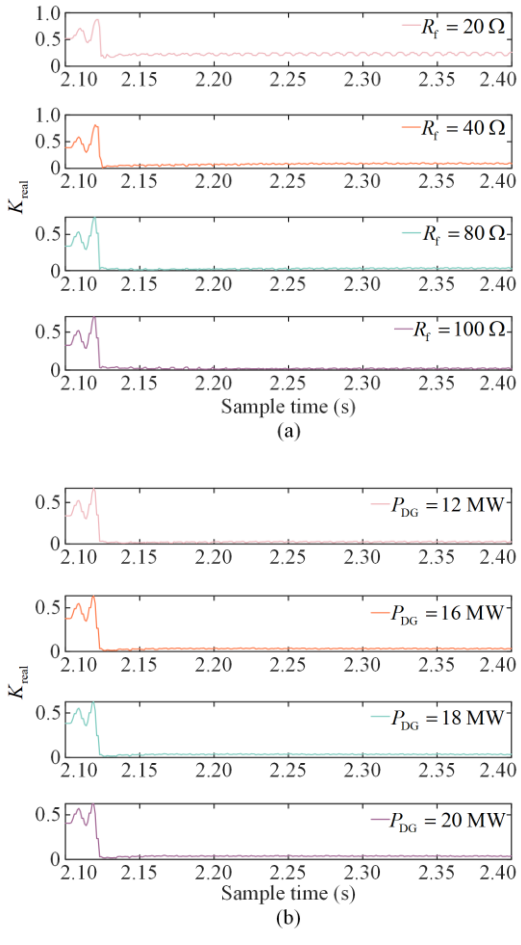

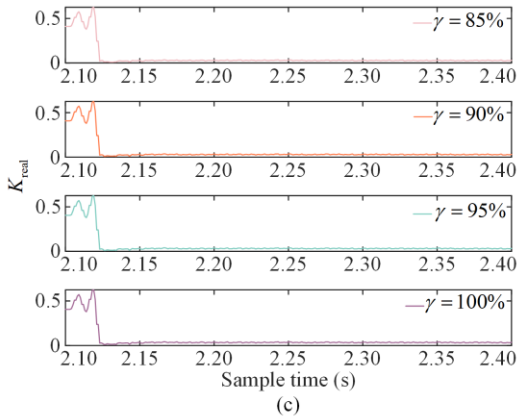

Fig. 19. K_{real} for cases 1-3. (a) Case 1. (b) Case 2. (c) Case 3.

2) Reverse Faults

Assume that a metallic SPGF occurs at bus N. The fault-phase current is shown in Fig. 20.

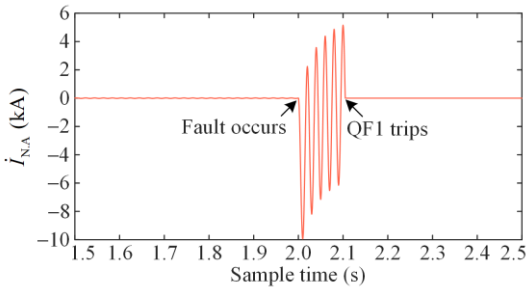

Fig. 20. $\dot{I}_{N.A}$ with the reverse fault.

In Fig. 20, the transient value of $\dot{I}_{N.A}$ reaches 10 kA during the fault stage. After QF1 trips, $\left|\dot{I}_{N.A}\right| = 0$ A , as there is no DG downstream of QF3, which concurs with the theoretical analysis in Section III. Then, the reverse fault can be effectively identified in the single-DG network. The following simulations in this section are all conducted in the multiple-DG network, as the fault characteristics in the single-DG network are relatively simple.

B. Validation for a T-type Network with Multiple DGs

In this sub-section, the effectiveness of the proposed scheme is validated for a multiple-DG network. The simulation parameters for cases 4–7 with different fault scenarios are listed in Table IV.

TABLE IV
SIMULATION PARAMETERS FOR CASES 4–7

Variable	R_f (Ω)	P_{L2} (MW)	P_{DG2} (MW)	λ (%)
Case 4	0.01,20,50,100	2	10	100
Case 5	10	2, 3, 4, 5	10	100
Case 6	100	2	12, 14, 16, 18	100
Case 7	50	2	10	100,95,90,85

Unlike the single-DG network, the DG is also connected to the downstream part of QF3 in this case. P_{DG1} is uniformly set as 4 MW, and P_{L1} is set as 4 MW in cases 4–7. In Tables V–VIII, the effectiveness of the proposed scheme is verified in the multiple-DG network in cases 4–7. Because the gap breakdown time is approximately 15 ms, the value of Z_{real} after QF1 tripped is adopted as 35 ms in this study.

TABLE V
ACTION PERFORMANCE FOR CASE 4

R_f (Ω)	Eq. (28) (Ω)	DPS-I?	Eq. (27) (Ω)	DPS-II?	K'_{real}
0.01	4.54	×	17.61	√	0.918
20	4.50	×	17.58	√	0.156
50	4.58	×	17.59	√	0.065
100	4.54	×	17.63	√	0.030

Note: √ means the DPS operates and × means the DPS does not to operate.

TABLE VI
ACTION PERFORMANCE FOR CASE 5

P_{L2} (MW)	Eq. (28) (Ω)	DPS-I?	Eq. (27) (Ω)	DPS-II?	K'_{real}
2	4.31	×	17.59	√	0.273
3	4.75	×	17.54	√	0.303
4	4.56	×	17.55	√	0.296
5	4.42	×	17.57	√	0.282

TABLE VII
ACTION PERFORMANCE FOR CASE 6

P_{DG2} (MW)	Eq. (28) (Ω)	DPS-I?	Eq. (27) (Ω)	DPS-II?	K'_{real}
12	4.54	×	17.60	√	0.031
14	4.51	×	17.61	√	0.030
16	4.76	×	17.53	√	0.034
18	4.70	×	17.57	√	0.032

TABLE VIII
ACTION PERFORMANCE FOR CASE 7

λ (%)	Eq. (28) (Ω)	DPS-I?	Eq. (27) (Ω)	DPS-II?	K'_{real}
85	4.13	×	17.65	√	0.026
90	4.25	×	17.60	√	0.029
95	4.17	×	17.66	√	0.026
100	4.36	×	17.59	√	0.030

1) Forward Faults

After using (26), Z_{real} becomes close to Z_{Nf} in all scenarios. $|Z_{real}| > |Z^{I}_{set.N}|$ is satisfied in cases 4–7, and DPS-I at QF2 correctly remains inoperative. $\left|Z_{real} - \frac{1}{2}Z^{II}_{set.N}\right| \leqslant \left|\frac{1}{2}Z^{II}_{set.N}\right|$ is satisfied in all scenarios by substituting Z_{real} with Z_N. The protection logic is altered from "0" to "1" within 15 ms after QF1 trips. The distance protection parameters $K'_{real} > 0$ is obtained for all scenarios, and the results validate the theoretical analysis. Thus, DPS-II at QF2 in the multiple-DG network can reliably operate.

2) Reverse Faults

To further verify the reliability of the proposed scheme in the multiple-DG network, the DPS performance is observed for revere faults. Assuming that SPGFs with different R_f occur at bus N, Z_{real} and K'_{real} for this scenario are displayed in Table IX.

TABLE IX
ACTION PERFORMANCE FOR REVERSE FAULTS

R_f (Ω)	Z_{real} (Ω)	K'_{real}	DPS-II?
0.01	–0.01-j0.03	–0.029	×
20	–0.09-j0.07	–0.041	×
50	–0.13-j0.11	–0.066	×
100	–0.33-j0.14	–0.098	×

In Table IX, K'_{real} is always less than 0 and Z_{real} is located in the fourth quadrant of the impedance circle, which implies that the fault direction is reverse. Thus, QF2 does not trip for reverse faults, verifying that the proposed scheme is capable of identifying fault direction.

C. Comparison of Action Performance for Different Protection Schemes

Considering an SPGF near QF1, the action performances of different protection schemes are observed. In Table X, R_f is set as 100 Ω; λ = 85%, 90%, 95%, and 100%; P_{DG} = 10 MW, 15 MW, and 20 MW; and P_L = 5 MW. Unlike in the traditional schemes in [33] and [34], the positive-sequence current distribution factor is replaced with the negative-sequence current distribution factor to express the fault information. This approach is unrelated to the fault characteristics of the DGs, extending its applicability to different networks.

As shown in Table X, schemes in [33] and [34] fail to satisfy the action criterion for some scenarios because $\left|Z_{real} - \frac{1}{2}Z^{II}_{set.N}\right| > \left|\frac{1}{2}Z^{II}_{set.N}\right|$. However, for the proposed scheme, QF2 can trip correctly because (27) is satisfied in all scenarios, thereby validating the superiority of the proposed scheme.

TABLE X
ACTION PERFORMANCE COMPARISON

Scheme	λ (%)	P_{DG} (MW)	Eq. (27) (Ω)	DPS-II?	QF2 trips?
Scheme [33]	85%	10	18.92	×	No
		15	17.88	√	Yes
		20	19.21	×	No
	90%	10	17.71	√	Yes
		15	17.53	√	Yes
		20	19.76	×	No
	95%	10	17.87	√	Yes
		15	18.94	×	No
		20	19.73	×	No
	100%	10	17.91	√	Yes
		15	19.45	×	No
		20	20.52	×	No
Scheme [34]	85%	10	17.69	√	Yes
		15	17.67	√	Yes
		20	18.75	×	No
	90%	10	17.73	√	Yes
		15	17.86	√	Yes
		20	19.05	×	No
	95%	10	17.73	√	Yes
		15	17.89	√	Yes
		20	19.14	×	No
	100%	10	17.95	√	Yes
		15	19.21	×	No
		20	19.77	×	No
This paper	85%	10	17.55	√	Yes
		15	17.69	√	Yes
		20	17.78	√	Yes
	90%	10	17.49	√	Yes
		15	17.57	√	Yes
		20	17.66	√	Yes
	95%	10	17.51	√	Yes
		15	17.59	√	Yes
		20	17.67	√	Yes
	100%	10	17.45	√	Yes
		15	17.49	√	Yes
		20	17.68	√	Yes

V. CONCLUSION

This paper investigates the effect of gap breakdown issues on DG side DPS in a gap-grounded system. First, the influencing factors of the measured impedance within T-type networks with gap-grounded systems are analyzed. Then, it delved into the theoretical implications of gap breakdown issues on the measured impedance. To assess the trend of the measured impedance, the ratio of the short-circuit currents at the protection locations of the DGs is defined. The theoretical analysis demonstrates that the traditional protection action criterion is difficult to satisfy, and DPS-II at the DG side may not operate. Therefore, this study proposes an enhanced DPS designed to mitigate the effect of gap breakdown. This scheme improves the traditional protection approach in T-type networks with a single DG and multiple DGs. The real short-circuit impedance is addressed to comply with the protection action criterion by utilizing the relationship between the phasors in the impedance circle.

To overcome the limitations of the traditional schemes, the positive-sequence distribution factor is replaced by the negative-sequence distribution factor to characterize the fault information. A simulation model of a T-type active distribution network with gap-grounded transformers is developed in PSCAD /EMTDC. The simulation results revealed that the calculated real short-circuit impedances across various fault scenarios align closely with the theoretical values, ensuring the protection action criterion is met. The effectiveness of the protection scheme is also confirmed. Moreover, the improved scheme accurately avoided tripping for reverse faults, thereby enhancing the protection reliability.

However, several areas require further research. For example, the coordination between the DG islanding protection and transmission line protection significantly influences the reliable and safe operation of the grid and DGs connected to distribution networks.

ACKNOWLEDGMENT

Not applicable.

AUTHORS' CONTRIBUTIONS

Wanqi Yuan: full-text writing, the construction of the paper framework, conceptualization, methodology, data curation, software, and original draft preparation. Yongli Li: supervision, reviewing, and editing. Xiaolong Chen: checked English expression, reviewing, and editing. Shaofan Zhang, Jing Wan, and Huili Tian: reviewing and editing. All authors read and approved the final manuscript.

FUNDING

This work is supported by the Science and Technology Project of China Southern Power Grid (No. 030108KK52222003).

AVAILABILITY OF DATA AND MATERIALS

Please contact the corresponding author for data material request.

DECLARATIONS

Competing interests: The authors declare that they have no known competing financial interests or personal relationships that could have appeared to influence the work reported in this paper.

AUTHORS' INFORMATION

Wanqi Yuan received the B.S. degree in the School of Internet of Things Engineering, Jiangnan University, Wuxi, China in 2017 and the Master's degree in the School of Electrical and Information Engineering, Tianjin University, Tianjin, China in 2022. He is currently pursuing a PhD degree in the School of Electrical and Information Engineering, Tianjin University. His current research interests include faulty phase selection and distributed generators accessed to the distribution networks.

Yongli Li received the B.Sc. and M.Sc. degrees in electrical engineering from Tianjin University, China, in 1984 and 1987, respectively. In 1993, she received the Ph.D. degree in electrical engineering from the Universite Libre de Bruxelles, Belgium. She is currently a professor with the School of Electrical and Information Engineering, Tianjin University. Her research interests include fault analysis of power systems and fault diagnosis of electrical equipment, protection, and adaptive reclosing of EHV/UHV transmission systems, and protection and control of the microgrids, HVDC, and distribution networks. Prof. Li is a member of CIGRE SC-B5.

Xiaolong Chen was born in Henan, China. He received the B.Sc., M.Sc., and Ph.D. degrees from Tianjin University, Tianjin, China, in 2010, 2012, and 2015, respectively, all in electrical engineering. From 2015 to 2019, he was a lecturer with the School of Electrical and Information Engineering, Tianjin University, where he has been an associate professor since 2019. His research interests include islanding detection for the microgrid, fault analysis and protection for active distribution power system, state monitoring and fault diagnosis of the breaker, and DC grid and hybrid DC grid protection and control.

Shaofan Zhang received a Bachelor's degree in Electrical Engineering from Shanghai Jiaotong University, Shanghai, China, in 1998. He joined Guangzhou Power Supply Bureau in 1998 and has been working in the field of relay protection since then. He Obtained the title of Senior Engineer in Power Engineering in 2018.

Jing Wan was born in Henan, China. She received the M.Sc. degree in electrical engineering from South China University of Technology, Guangzhou, China, in 2020. She is currently working at the Guangzhou Power Supply Bureau since 2020. Her research interest is dispatching automation of power gird.

Huili Tian received a Master's degree in Electrical Engineering from Xi'an Jiaotong University, Xi'an China, in 2011. She joined Guangzhou Power Supply Bureau in 2011 and has been working in the field of distribution network dispatch and operation since then. She Obtained the title of Senior Engineer in Power Engineering in 2021.

REFERENCES

[1] Y. Liang, K. J. Li, and Z. Ma *et al*., "Multilabel classification model for type recognition of single-phase-to-ground fault based on KNN-Bayesian method," *IEEE Transactions on Industry Applications*, vol. 57, no. 2, pp. 1294-1302, Mar. 2021.

[2] C. Galvez and A. Abur, "Fault location in active distribution networks containing distributed energy resources (DERs)," *IEEE Transactions on Power Delivery*, vol. 36, no. 5, pp. 3128-3139, Oct. 2021.

[3] S. Liu, J. Liu, and X. Li, *et al*., "Single-terminal travelling wave based fault location method in t-type transmission line," in *2022 IEEE/IAS Industrial and Commercial Power System Asia (I&CPS Asia)*, Shanghai, China, 2022, pp. 427-432.

[4] F. Debrue, C. Gonzalez, and T. Wijnhoven *et al*., "Influence of distributed generation on the protection principles of a 70 kV/15 kV transformer in antenna: the zero-sequence overvoltage protection U0," in *IET International Conference on Developments in Power System Protection*, Copenhagen, Denmark: IET, 2014: 48.

[5] R. Shen, Z. Han, and S. Liu *et al*.,"A novel distance protection method for out-of-phase faults of AC traction power supply system," *IEEE Transactions on Power Delivery*, vol. 38, no. 5, pp. 3729-3732, Oct. 2023.

[6] Q. Lai, Z. Zhang, and J. Han *et al*., "Research on neutral grounding mode of interconnecting transformer in renewable energy plant," *IEEE Transactions on Power Delivery*, vol. 37, no. 5, pp. 4166-4177, Qct. 2022.

[7] K. Jia, Z. Wang, and M. Dai *et al*., "Influence of distributed PV integration on neutral point voltage of 110 kV main transformer," *Electric Power Automation Equipment*, vol. 38, no. 11, pp. 181-186, Nov. 2018. (in Chinese)

[8] T. Yuan, H. Gao, and F. Peng *et al*., "Adaptive quasi-power differential protection scheme for active distribution networks," *IEEE Transactions on Smart Grid*, vol. 15, no. 1, pp. 324-339, Jan. 2024.

[9] K. T. Martin, A. C. Marchesan, and O. C. B. de Araújo *et al*., "Mixed integer linear programming applied to adaptive directional overcurrent protection considering *N*-1 contingency," *IEEE Transactions on Industry Applications*, vol. 59, no. 3, pp. 2807-2821, May 2023.

[10] U. U. Uma, D. Nmadu, and N. Ugwuanyi *et al*., "Adaptive overcurrent protection scheme coordination in presence of distributed generation using radial basis neural network," *Protection and Control of Modern Power Systems*, vol. 8, no. 4, pp. 1-19, Oct. 2023.

[11] H. Sadeghi, "A novel method for adaptive distance protection of transmission line connected to wind farms," *International Journal of Electrical Power and Energy Systems*, vol. 43, no. 1, pp. 1376-1382, Dec. 2012.

[12] B. Bhalija and R. P. Maheshwari, "An adaptive distance relaying scheme using radial basis function neural net-

work, " *Electric Power Components and Systems*, vol. 35, no. 3, pp. 245-259, Feb. 2007.
[13] M. Sanaye-Pasand and P. Jafarian, "An adaptive decision logic to enhance distance protection of transmission lines, " *IEEE Transactions on Power Delivery*, vol. 26, no. 4, pp. 2134-2144, Oct. 2011.
[14] J. Ma, W. Ma, and Y. Qiu, *et al*., "An adaptive distance protection scheme based on the voltage drop equation," *IEEE Transactions on Power Delivery*, vol. 30, no. 4, pp. 1931-1940, Aug. 2015.
[15] Y. Liang, W. Li, Z. Lu *et al*., "A new distance protection scheme based on improved virtual measured voltage," *IEEE Transactions on Power Delivery*, vol. 35, no. 2, pp. 774-786, Apr. 2020.
[16] G. Song, X. Chu, and S. Gao *et al*., "Novel distance protection based on distributed parameter model for long-distance transmission lines, " *IEEE Transactions on Power Delivery*, vol. 28, no. 4, pp. 2126-2123, Oct. 2013.
[17] Z. Xu, S. Jiang, and Q. Yang *et al*., "Ground distance relaying algorithm for high-resistance fault," *IET Generation*, *Transmission & Distribution*, vol. 4, no. 1, pp. 27-35, Jan. 2010.
[18] Z. Xu, G. Xu, and L. Ran *et al*., "A new fault-impedance algorithm for distance relaying on a transmission line," *IEEE Transactions on Power Delivery*, vol. 25, no. 3, pp. 1384-1392, Jul. 2010.
[19] V. H. Makwana and B. R. Bhalja, "Distance relaying algorithm for a line-to-ground fault on single infeed lines," *Electric Power Components and Systems*, vol. 42, pp. 1227-1238, Jul. 2014.
[20] V. H. Makwana and B. R. Bhalja, "A new digital distance relaying scheme for compensation of high-resistance faults on transmission line," *IEEE Transactions on Power Delivery*, vol. 27, no. 4, pp. 2133-2140, Oct. 2012.
[21] Y. Liang, Y. Huo, and F. Zhao, "An accelerated distance protection of transmission lines emanating from MMC-HVDC stations," *IEEE Journal of Emerging and Selected Topics in Power Electronics*, vol. 9, no. 5, pp. 5558-5570, Oct. 2021.
[22] Y. Liang, W. Li, and W. Zha, "Adaptive Mho characteristic-based distance protection for lines emanating from photovoltaic power plants under unbalanced faults," *IEEE Systems Journal*, vol. 15, no. 3, pp. 3506-3516, Sept. 2021.
[23] A. Zhang, K. Qian, F. Huang *et al*., "Analysis on influence of neutral point grounded through gap in transformer with distributed wind power on distance protection and its countermeasures, " *Smart Power*, vol. 49, no. 9, Sept. 2021. (in Chinese)
[24] W. Ou and B. Ye, "Reliability analysis of typically connection modes in HV distribution network," *High Voltage Engineering*, vol. 32, no. 2, pp. 106-107, Feb. 2006. (in Chinese)
[25] G. Wan, W. Liu, and S. Chen, "Study on pertinent issues of 3T-conection mode of the 110 kV power grid," *Power System Technology*, vol. 31, No. S2, pp. 360-362, Dec. 2007. (in Chinese)
[26] B. Mallikarjuna, P. Shanmukesh, and D. Anmol *et al*., "PMU based adaptive zone settings of distance relays for protection of multi-terminal transmission lines," *Protection and Control of Modern Power Systems*, vol. 3, no. 2, pp. 1-15, Apr. 2018.
[27] J. C. Quispe and E. Orduña, "Transmission line protection challenges influenced by inverter-based resources: a review," *Protection and Control of Modern Power Systems*, vol. 7, no. 3, pp. 1-17, Jul. 2022.
[28] "Technical specification for neutral point overvoltage protection of 220 kV and 110 kV transformers," *Beijing: China Electric Power Press*, 2018.
[29] C. He, R. Qin, and B. Xu *et al*., "Influence of distributed generation on power frequency overvoltage characteristics of transformer neutral point," in *2022 12th International Conference on Power and Energy Systems (ICPES)*, Guangzhou, China, pp. 210-213, 2022.
[30] A. Ghorbani1, S. Y. Ebrahimi, and M. Ghorbani, "Active power based distance protection scheme in the presence of series compensators," *Protection and Control of Modern Power Systems*, vol. 2, no. 1, pp. 1-13, Jan. 2017.
[31] L. He, Y. Li, and X. Chu *et al*., "Single-phase to ground fault line identification for medium voltage islanded microgrids with neutral ineffectively grounded modes," *IEEE Transactions on Smart Grid*, vol. 13, no. 6, pp. 4312-4326, Nov. 2022.
[32] C. Chao, X. Zheng, and Y. Weng *et al*., "Adaptive distance protection based on the analytical model of additional impedance for inverter-interfaced renewable power plants during asymmetrical faults," *IEEE Transactions on Power Delivery*, vol. 37, no. 5, pp. 3823-3834, Oct. 2022.
[33] Y. Liang, Z. Lu, and W. Li *et al*., "A novel fault impedance calculation method for distance protection against fault resistance," *IEEE Transactions on Power Delivery*, vol. 35, no. 1, pp. 396-407, Jan. 2020.
[34] X. Chen, W. Qin, and L. Yang *et al*., "Adaptive distance protection scheme for a distribution network given access of inverter power supply," *Power System Protection and Control*, vol. 51, no. 11, pp. 27-38, Jun. 2023. (in Chinese)